ME 69-T57-2

The University of Tennessee

Department of Mechanical and Aerospace Engineering

AN EXPERIMENTAL STUDY OF THE VISCOSEAL BEARING

by

Chandrakant Khumaji Shah

Supported by

NATIONAL AERONAUTICS AND SPACE ADMINISTRATION

DEPARTMENT OF DEFENSE

Prepared Under

NASA Grant NGR-43-001-003

February 1969

Knoxville, Tennessee 37916

FOREWARD

This document is submitted as an interim report on the viscoseal which is part of the University of Tennessee Dynamic Sealing research program. Support for this work was provided by contract N00014-68-A-0144 with the Office of Naval Research and grant NGR-43-001-003 from the National Aeronautics and Space Administration.

This report was submitted to the University of Tennessee in partial fulfillment of the requirements for the degree Master of Science and is presented here with minor changes in format.

The author wishes to express appreciation to Professor W. K. Stair of the Department of Mechanical and Aerospace Engineering for his guidance and assistance in preparation of this report.

Special appreciation is extended to the author's family, whose patience, understanding and encouragement helped him to achieve his educational goal.

Approved: _____ _____

W. K. Stair C. K. Shah

ABSTRACT

The experimental data obtained from two groove geometries of the viscoseal bearing were analysed to study the bearing characteristics and the sealing performance. The experimental bearing characteristics were compared with the Dubois and Ocvirk Short-bearing Approximation. The sealing performance analysis of the bearing included (1) the determination of the sealing coefficient which was compared with the Stair and Hale method of theoretical prediction and (2) the effect of the bearing eccentricity ratio on the sealing coefficient, which was compared with the Vohr and Chow method of theoretical prediction.

The results of the study indicated that, at constant load and speed, the bearing supply pressure had no effect on the bearing eccentricity ratio; at a constant flow rate, however, the bearing supply pressure decreased as the bearing eccentricity ratio increased. Except for the shaft center locus findings, the experimental results were in fair agreement with the Short-bearing Approximation. The experimental results showed good agreement with a numerical analysis of the viscoseal bearing. The study also indicated that an increase in the land width resulted in an increase in the load-carrying capacity of the bearing. The experimental sealing coefficient did not agree with the theoretical prediction, although the results indicated that the sealing coefficient increased with an increase in the bearing eccentricity ratio.

TABLE OF CONTENTS

CHAPTER		PAGE
I.	INTRODUCTION	1
II.	EXPERIMENTAL APPARATUS AND TEST PROCEDURE	12
	Test Bearing Assembly	12
	Film Thickness Measurement	12
	Friction Torque Measurement	15
	Temperature Measurement	18
	Oil Flow Measurement	18
	Properties of Gulf Harmony 47 Oil	19
	Test Procedure	21
III.	RESULTS ON BEARINGS NO. 1 and NO. 2	24
IV.	DISCUSSION AND CONCLUSIONS	39
LIST OF REFERENCES		46
APPENDIXES		48
	A. SAMPLE CALCULATIONS AND DATA SHEET	49
	B. CALIBRATION OF FILM THICKNESS MEASUREMENT DEVICE	56
	C. CALIBRATION OF TORQUE BEAM	59
	D. CALIBRATION OF FLOW METER	61
VITA		64

LIST OF TABLES

TABLE		PAGE
I.	Details of Test Series on Bearing No. 1	22
II.	Details of Test Series on Bearing No. 2	23
III.	Percentage Load-Carrying Capacity of Bearing No. 1	33
IV.	Percentage Load-Carrying Capacity of Bearing No. 2	34
V.	Theoretical and Experimental Capacity Number for a Plain Journal Bearing by Dubois and Ocvirk	40
VI.	Experimental and Theoretical Load-Carrying Capacities of Bearing No. 1	43
VII.	Sample Data Sheet	50

LIST OF FIGURES

FIGURE		PAGE
1.	Basic Elements of the Viscoseal	2
2.	Elements of the Viscoseal Bearing	7
3.	Geometries No. 1 and No. 2 of Viscoseal Bearing	8
4.	Test Bearing Assembly	13
5.	Hydraulic System Schematic	14
6.	Eccentricity Measuring System Schematic	16
7.	Torque-Beam Assembly	17
8.	Viscosity Versus Temperature on ASTM Type B Chart	20
9.	Bearing Supply Pressure Versus Eccentricity Ratio at Constant Load and Constant Speed	25
10.	Bearing Supply Pressure Versus Eccentricity Ratio at Constant Flow Rate	26
11.	Eccentricity Ratio Versus Attitude Angle	27
12.	Capacity Number Versus Eccentricity Ratio	28
13.	Load Number Versus Friction Ratio	29
14.	Capacity Number Versus Friction Variable	30
15.	Reynolds Number Versus Sealing Coefficient	36
16.	Flow Rate Versus $\Delta p/\mu$	37
17.	Eccentricity Ratio Versus Sealing Coefficient	38
18.	Influence of a Circumferential Groove upon the Axial Pressure Distribution in the Oil Film (a) Bearing With One Groove; (b) Bearing With Three Grooves	41

FIGURE PAGE

19. Relative Position of Sensing Elements at the Time of Calibration 57

20. Distance Detector Voltage Output Versus Bearing Clearance 58

21. Load Versus Strain on the Torque Beam 60

22. Float Characteristic Curves Reproduced from the Catalog by Fischer and Porter, Tri-flat Variable-Area Flowmeters, Handbook 10A9010, Warminster: Fischer and Porter Co., January 1964 62

LIST OF SYMBOLS

SYMBOL	DESCRIPTION	UNIT
English Alphabet		
a	Axial land width	inch
A	Size factor for flow meter	
b	Axial groove width	inch
B	Size factor for flow meter	
c	Radial clearance	inch
c_d	Diametral clearance	inch
C	Flow coefficient	
Cn	Capacity number = $(\mu N'/p')(d/c_d)^2(\ell/d)^2$	dimensionless
d	Seal diameter or bearing diameter	inch
f	Friction coefficient = F/W	dimensionless
F	Circumferential bearing friction force under load, W	lb.
Fo	Circumferential bearing friction force at zero load	lb.
Fv	Friction variable	dimensionless
h	Groove depth	inch
H	Local film thickness	inch
ℓ	Bearing length or axial threaded length of seal	inch
L	Seal length	inch
m	Number of grooves	

SYMBOL	DESCRIPTION	UNIT
N	Shaft speed	RPM
N'	Shaft speed = N/60	RPS
n	Number of thread starts	
p	Pressure	$lb_f/inch^2$
Δp	Pressure difference along seal length, L	$lb_f/inch^2$
p'	Unit load	$lb_f/inch^2$
Q	Flow rate	Std cc/min
R	Viscous influence number	
Re_c	Reynolds number based on clearance = Uc ρ/μ	dimensionless
t	Tangent of helix angle	dimensionless
U	Surface velocity of shaft	inch/sec
W	Total load or load-carrying capacity	lb.
x	Coordinate in the direction of motion	
y	Coordinate along axis of shaft	
z	Coordinate normal to moving surface	

Greek Alphabet

α	Helix angle of viscoseal or viscoseal bearing	degree
β	$(h + c)/c$	dimensionless
γ	$b/(a + b)$	dimensionless
ε	Eccentricity ratio	dimensionless
ξ	Coordinate along groove	
η	Coordinate normal to groove axis	

SYMBOL	DESCRIPTION	UNIT
Λ	Sealing coefficient = $6\mu UL/c^2\Delta p$	dimensionless
μ	Absolute viscosity	lb_f-sec/inch^2
ρ	Density	gm/cc or lb_m/inch^3
τ	Wall shearing stress	lb_f/inch^2
ϕ	Attitude angle	degree

Subscripts

E	denotes experimental
T	denotes theoretical or Short-bearing Approximation
VB	denotes viscoseal bearing
JB	denotes journal bearing
f	denotes float
OPT	denotes operating pressure and temperature
STP	denotes standard pressure and temperature
1	denotes Bearing No. 1
2	denotes Bearing No. 2.

CHAPTER I

INTRODUCTION

This thesis is concerned with the continued development of the viscoseal as a bearing.

The viscoseal is a device in which a pressure gradient is generated in a viscous fluid enclosed in a thin annulus or slit by means of grooves on a rotating shaft or plate. Such a device is known as a viscopump if operating with a net efflux of fluid at the high pressure end, and as a viscoseal when operating at shut-off head. Figure 1 describes the basic elements of the viscoseal. While one of the earliest treatments of the viscoseals was published in 1924 [1],[1] technological development of the viscoseal has been exploited only in recent years [2, 3, 4, 5, 6].

Previous work [2] reported that the viscoseal would sustain a radial load which was approximately 12 to 15 per cent of the capacity of a plain journal bearing of the same overall dimensions. The obvious reason for reduced capacity is that grooves interrupt the active length of the bearing and divide the bearing into a number of short bearings, each having a low length-to-diameter ratio. However, the viscoseal has sufficient bearing-load capacity to give it utility in certain high speed, low load applications.

---

[1] Numbers appearing in brackets refer to references listed in reference section.

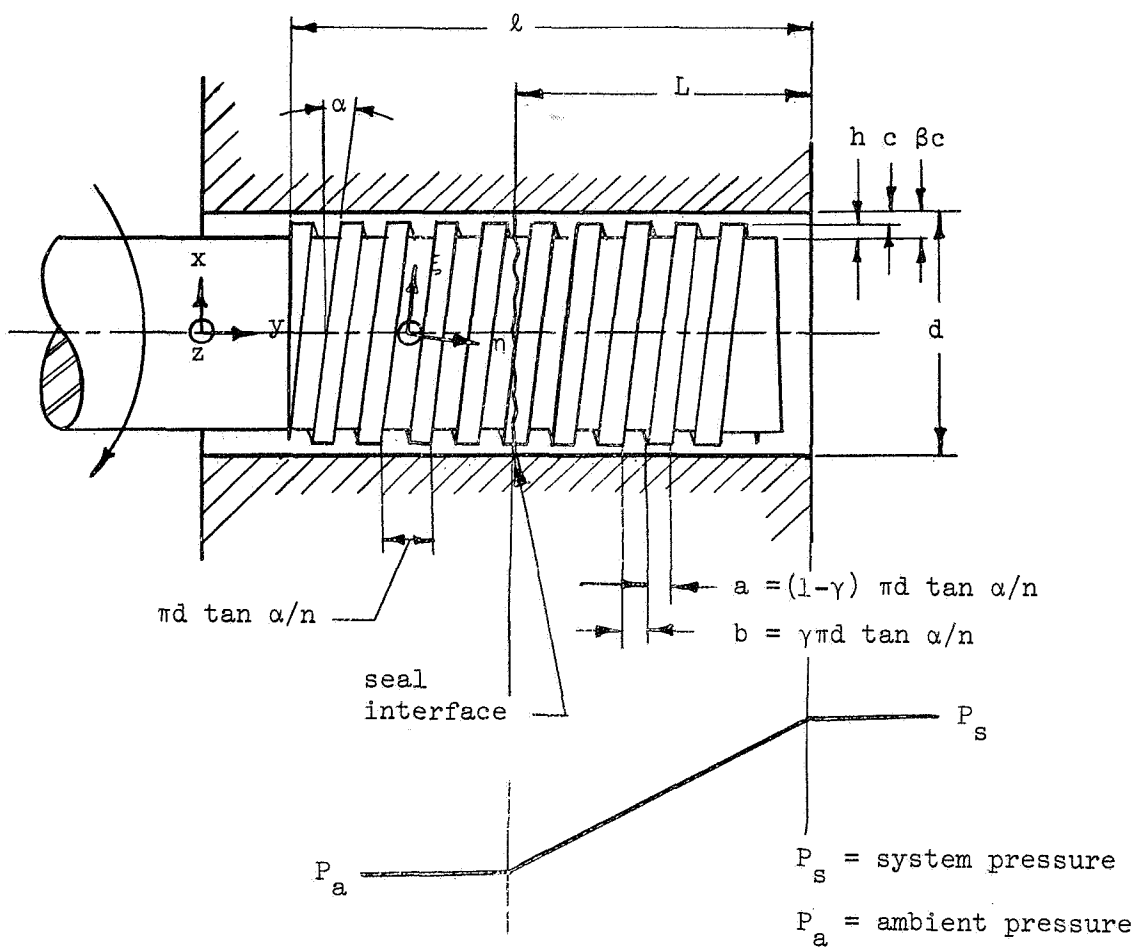

Figure 1. Basic elements of the viscoseal.

A general equation [3] for the sealing performance of the visco-seal in laminar and turbulent operations has been developed as follows:

$$\Lambda = \frac{6\mu\, UL}{c^2\, \Delta p} \quad . \qquad (1)^1$$

Of several analyses discussed in [3], the work of Boon and Tal shows the best agreement with experiment. The equation for the laminar sealing coefficient derived by Boon and Tal [3] is:

$$\Lambda = \frac{\beta^3(1 + t^2) + t^2\gamma(1 - \gamma)(\beta^3 - 1)^2}{t\,\gamma(1 - \gamma)(\beta^3 - 1)(\beta - 1)} \quad , \qquad (2)$$

which shows that the laminar sealing coefficient is a function of groove geometry and independent of Reynolds number. The equation for the turbulent concentric sealing coefficient derived by Stair and Hale [4] is:

$$\Lambda = K_4 \left(\frac{I_1 + I_2}{I_4}\right) + K_5 \frac{I_3}{I_4} \quad , \qquad (3)$$

where

$$I_1 = (1 - \gamma)\, t^2 \quad , \qquad (4)$$

$$I_2 = \beta^3 \gamma\, t^2 \quad , \qquad (5)$$

$$I_3 = \frac{\beta^3}{[\gamma + \beta^3(1 - \gamma)]} \quad , \qquad (6)$$

---

[1] Numbers appearing in parentheses refer to equations.

$$I_4 = t\left[1 - \gamma + \gamma\beta - \frac{\gamma + \beta^3(1-\gamma) + \gamma(\beta - 1)}{\gamma + \beta^3(1 - \gamma)}\right], \quad (7)$$

$$K_4 = \frac{3}{2F_\xi}\left[1 - \frac{F_\xi}{10.5F_\xi - 7.5} + \frac{1 - F_\xi}{3.92F_\xi^2 - 1.4F_\xi - 1}\right], \quad (8)$$

and

$$K_5 = \frac{3}{2F_\eta}\left[1 - \frac{F_\eta}{10.5F_\eta - 7.5} + \frac{1 - F_\eta}{3.92F_\eta^2 - 1.4F_\eta - 1}\right]. \quad (9)$$

Here, F_ξ and F_η are the ratios of the wall shearing stress in turbulent flow to the wall shearing stress for laminar flow, with the same maximum channel velocity. Thus,

$$F_\xi = (\tau_0/\tau_\ell)_\xi = (f_0/f_\ell)_\xi , \quad (10)$$

and

$$F_\eta = (\tau_0/\tau_\ell)_\eta = (f_0/f_\ell)_\eta . \quad (11)$$

Here, f_0 and f_ℓ are the resistance coefficients for turbulent and laminar operations respectively. From [4], the critical Reynolds number at which transition from laminar to turbulent operation occurs is:

$$Re = 41.1\left[\frac{D/2}{(1 - \gamma)c + \gamma\,\beta c}\right]^{1/2} . \quad (12)$$

An analysis of the viscoseal in turbulent operation suitable for eccentric as well as concentric operations was performed by Vohr and Chow [6]. Their equation for the sealing coefficient, which is based on a spiral-grooved screw seal, is:

$$\psi \equiv \frac{\partial p}{\partial y}\frac{c^2}{\mu U} = \left[\frac{0.5\gamma\, t(1-\gamma)(\beta-1)(\beta^3 G_{yg} - G_{yr})}{\beta^3 G_{yr}G_{yg} + t^2\gamma(1-\gamma)\, G_{yr}G_{xr} + \beta^3 t^2(1-\gamma)^2 G_{yr}G_{xg}}\right.$$

$$\left.\frac{}{+\,\gamma^2\beta^3\, t^2\, G_{yg}G_{xr} + \beta^6 t^2\, \gamma(1-\gamma)\, G_{yg}G_{xg}}\right], \qquad (13)$$

where subscripts x, y, z are the directions of coordinate axes, r and g indicate land and groove regions, and G_x and G_y are turbulent flow correction factors which depend on the Reynolds number based on surface velocity $UH\rho/\mu$, the dimensionless pressure gradient $H^3\,\Delta p\rho/\mu^2$, and the included angle between the directions of the pressure gradient and the direction of the surface velocity. The authors indicate, however, that for the conditions that prevail in a viscoseal, G_x and G_y may be generally considered to be functions of the Reynolds number $UH\,\rho/\mu$ alone. With the Reynolds number varying from 1000 to 100,000, the value of G_x in turn varies from 0.056 to 0.0024 and the value of G_y varies from 0.067 to 0.0025. The analysis also indicates that the sealing coefficient, Λ, increases as the eccentricity ratio increases. The ratio of the sealing coefficient at 0.9 eccentricity ratio to the

concentric sealing coefficient was found to be 1.35 for a Reynolds number of 1000 [6].

The viscoseal bearing, as the name implies, is a combination of a viscoseal and a journal bearing as shown in Figure 2. This report describes the experimental study of two different groove geometries of the viscoseal bearing, hereafter to be called Bearings No. 1 and No. 2. The critical Reynolds numbers for Bearings No. 1 and No. 2, the geometries of which are tabulated in Figure 3, were found from Equation (12) to be 449 and 548 respectively. The highest Reynolds number encountered in the experiment was less than 40. Thus, the study envisaged laminar operation only. The results obtained from the study have been analyzed with respect to bearing characteristics and sealing performance. The theoretical predictions for sealing performance were obtained from Equations (2) through (13). The equations for bearing characteristics were obtained from the Short-bearing Approximation [7], which is considered in the following paragraph:

From Figure 2, it is observed that the viscoseal bearing having m number of grooves can be considered as composed of m short bearings. Thus, the length-to-diameter ratio of each short bearing is given as a/d. Therefore, the results were calculated for a bearing having length-to-diameter ratio, a/d, and compared with the Short-bearing Approximation for the same ratio. The analytical and experimental investigation of the Short-bearing Approximation was conducted by Dubois and Ocvirk [7], who considered the following Reynolds' equation:

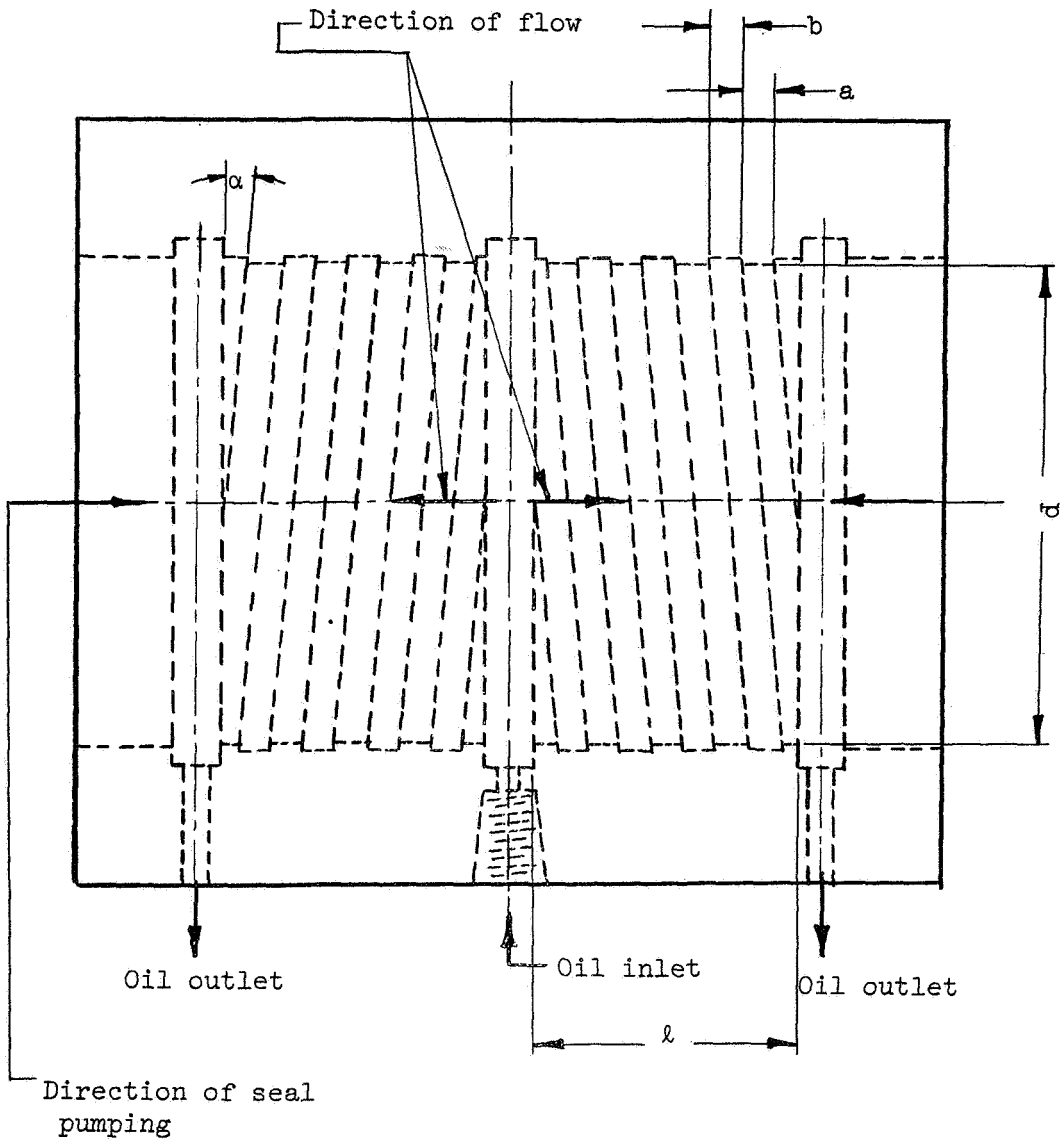

Figure 2. Elements of the viscoseal bearing.

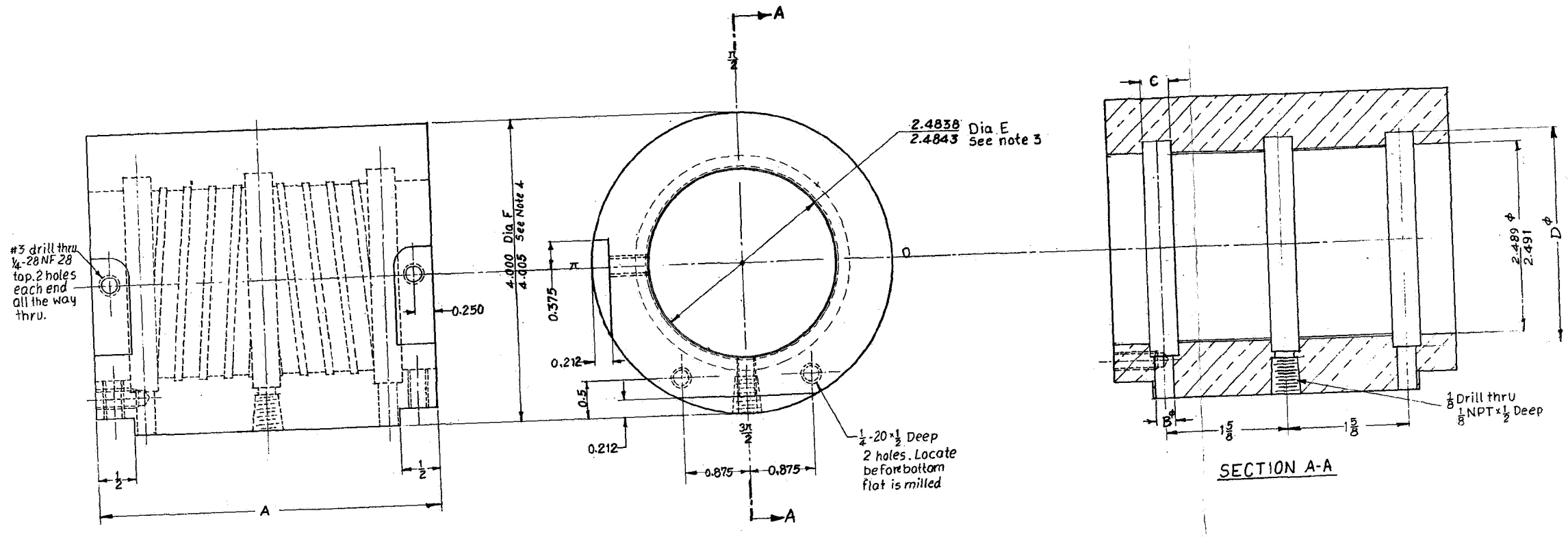

SECTION A-A

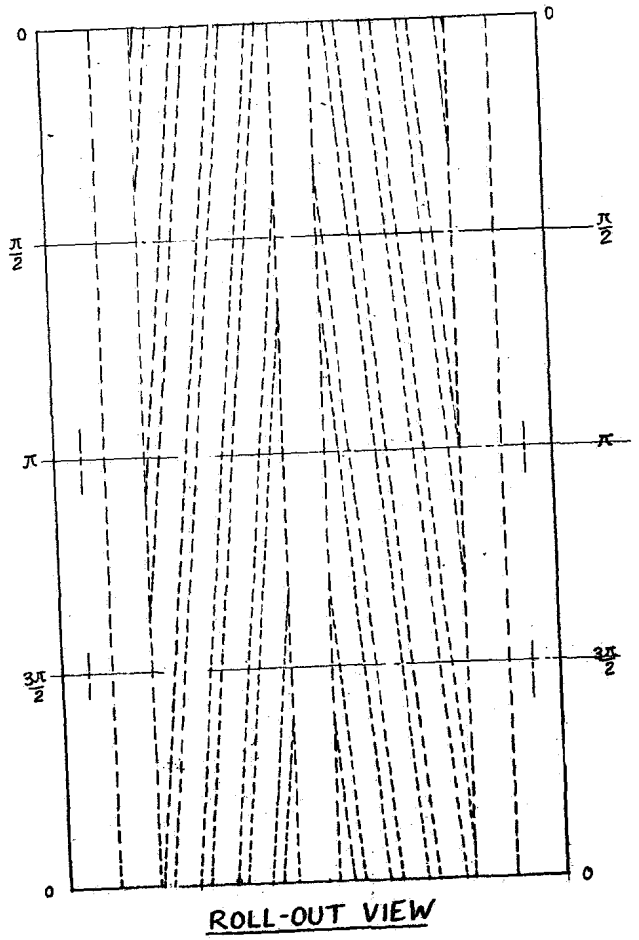

ROLL-OUT VIEW

	A	B	C	D	a	b	γ	α	h	n
Execution 1	4.5	⅛	0.25	2.735	0.1667	0.1667	0.5	4.88°	0.015	2
Execution 2	4.563	¼	0.375	2.859	0.2330	0.1000	0.3	4.88°	0.015	2

NOTES:

1. Internal Right Hand and Left Hand threads, to be cut symmetrical as shown in roll out view. First groove must start as shown within ± 0.001
2. Start first groove at 0 and π
3. Bore dia 'E' about 0.006 under size, cut threads, then hone to given dimensions
4. Dia 'E' must be concentric with dia 'F' within 0.001 TIR
5. Dia 'F' to be lapped
6. Tolerances UOS:
   3 place decimals ± 0.001
   2 place decimals ± 0.005

Figure 3. Geometries No. 1 and No. 2 of Viscoseal Bearing.

$$\frac{\partial}{\partial x}\left(\frac{H^3}{6\mu}\frac{\partial p}{\partial x}\right) + \frac{\partial}{\partial y}\left(\frac{H^3}{6\mu}\frac{\partial p}{\partial y}\right) = U\frac{\partial H}{\partial x} \quad . \tag{14}$$

The authors derived the following equations for the circumferential and endwise flow rates:

$$Q_x = \left(\frac{UH}{2} - \frac{H^3}{12\mu}\frac{\partial p}{\partial x}\right) dy \quad , \tag{15}$$

and

$$Q_y = \left(-\frac{H^3}{12\mu}\frac{\partial p}{\partial y}\right) dx \quad . \tag{16}$$

The principal simplifying assumption made by the authors was that, of the two right-hand terms in Equation (15), the second is negligible compared with the first. Therefore, Dubois and Ocvirk assumed that

$$Q_x = \frac{UH}{2} dy \quad . \tag{17}$$

Thus, this analytical approximation includes the endwise flow caused by $\partial p/\partial y$ and that part of the circumferential flow which is related to the surface velocity and local film thickness. This assumption results eventually in the omission of the first of the left-hand terms in Reynolds' equation (14). With this assumption, the authors solved Equation (14) and made available all the bearing characteristics and verified them experimentally for length-to-diameter ratios 1, $\frac{1}{2}$, and $\frac{1}{4}$, by the development of equations for load-carrying capacity, W ,

capacity number, Cn, attitude angle, ϕ , friction ratio, F/Fo , and friction variable, Fv, as follows:

$$W = \frac{\mu U \ell^3}{4c^2} \frac{\varepsilon}{(1-\varepsilon^2)^2} [\pi^2 (1-\varepsilon^2) + 16\varepsilon^2]^{1/2} , \tag{18}$$

$$Cn \equiv \frac{\mu N'}{p'} (\frac{d}{c_d})^2 (\frac{\ell}{d})^2 = \frac{(1-\varepsilon^2)^2}{\pi\varepsilon} [\frac{1}{\pi^2(1-\varepsilon^2) + 16\varepsilon^2}]^{1/2} , \tag{19}$$

$$\tan \phi = \frac{\pi}{4} \frac{(1-\varepsilon^2)^{1/2}}{\varepsilon} , \tag{20}$$

$$\frac{F}{Fo} \equiv \frac{F}{2\pi^2 \mu \, d\ell \, N'(d/c_d)} = \frac{1}{(1-\varepsilon^2)^{1/2}} , \tag{21}$$

$$Fv \equiv f(d/c_d)(\ell/d)^2 = Cn \frac{2\pi^2}{(1-\varepsilon^2)^{1/2}} . \tag{22}$$

The purpose of this project was to study the viscoseal bearing in the following ways:

1. To investigate the effect of the bearing eccentricity ratio on the bearing supply pressure. Results obtained from previous work [2] indicated that the bearing eccentricity ratio increased with an increase in the bearing supply pressure, for data taken at a constant load of 164.5 lb. and a constant speed of 1275 RPM with various supply pressures.

2. To study the bearing characteristics and the sealing performance of the viscoseal bearing.

3. To determine the possibility of increasing the bearing performance by changing groove geometry without having a significant reduction in the seal effectiveness.

CHAPTER II

EXPERIMENTAL APPARATUS AND TEST PROCEDURE

I. TEST BEARING ASSEMBLY

Test Bearings No. 1 and No. 2, which were constructed with a central supply groove, had pumping lands of opposite hand pumping toward the supply groove. The bearings were made of brass, and the shaft was made of type 316 stainless steel. Measurements of the shaft diameter and the diametral clearances for Bearings No. 1 and No. 2 were found to be 2.479, 0.0052 and 0.005 inches, respectively. The dimensions and the groove geometries of the bearings are described in Figure 3, page 8. Figure 4 indicates the manner in which the test elements were supported and loaded. The compound-wound D. C. motor used to drive the test equipment could be run at speeds ranging from 600 to 3400 RPM through the use of an armature control speed regulator. The hydraulic system for the test equipment is illustrated in Figure 5. Gulf Harmony 47 oil, which is similar to SAE 10 oil, was used for the loading pad as well as the lubrication of the bearings. The bearings had a groove on each end, in which oil drain holes were located. The oil drained from the bearings was pumped back to the supply tank where it was cooled by a water heat exchanger before being returned to the bearings.

II. FILM THICKNESS MEASUREMENT

Four inductance type transducers were used to measure the bearing film thickness which would determine the shaft center locus and

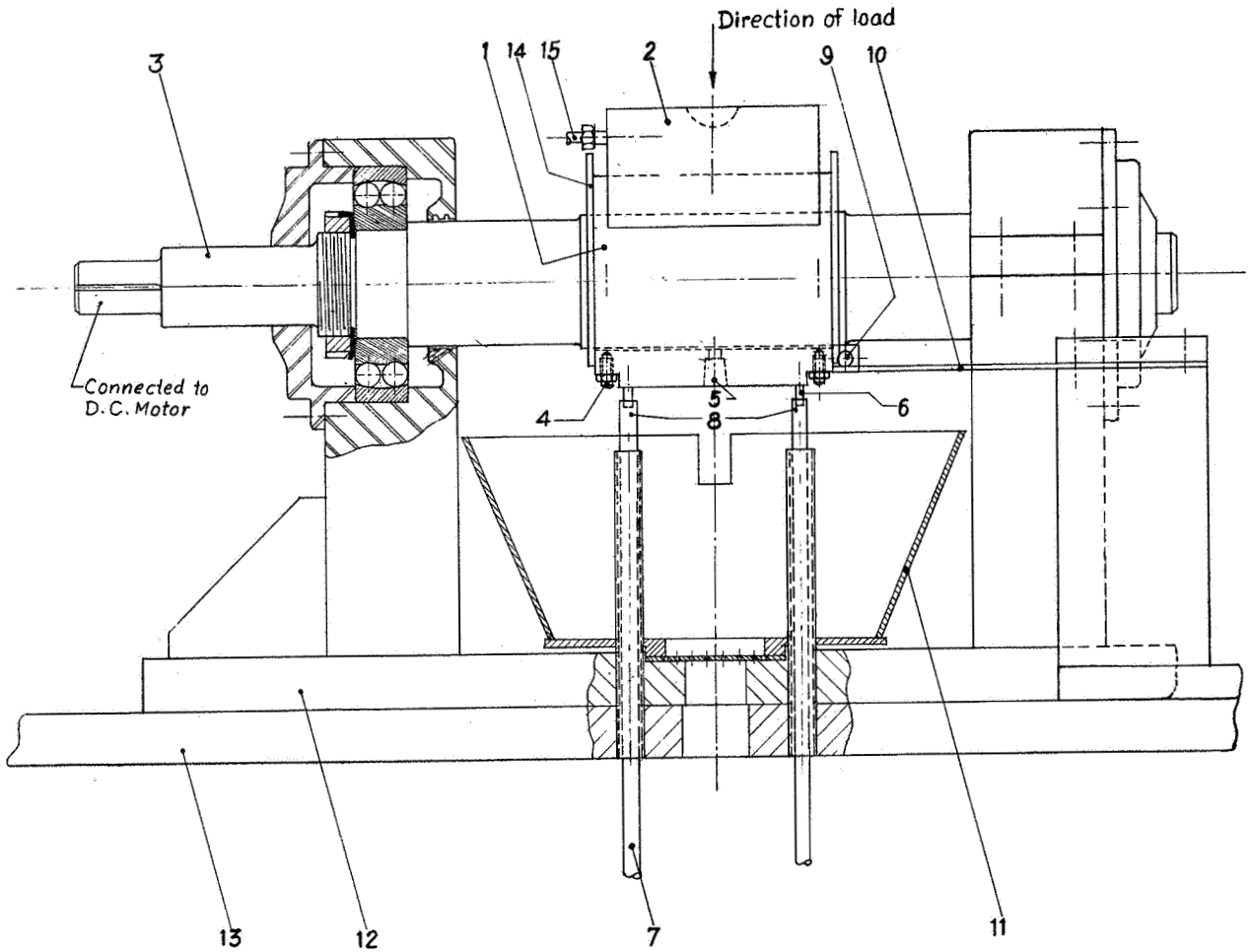

No.	NAME
15	Oil inlet to loading pad
14	End plate
13	Cast iron table
12	Base plate
11	Splash pan
10	Torque beam
9	Torque arm
8	Thermocouple
7	Drain pipe
6	Drain tube
5	Oil supply inlet
4	Clearance probe
3	Drive shaft
2	Hydrostatic loading pad
1	Test bearing

Figure 4. Test bearing assembly.

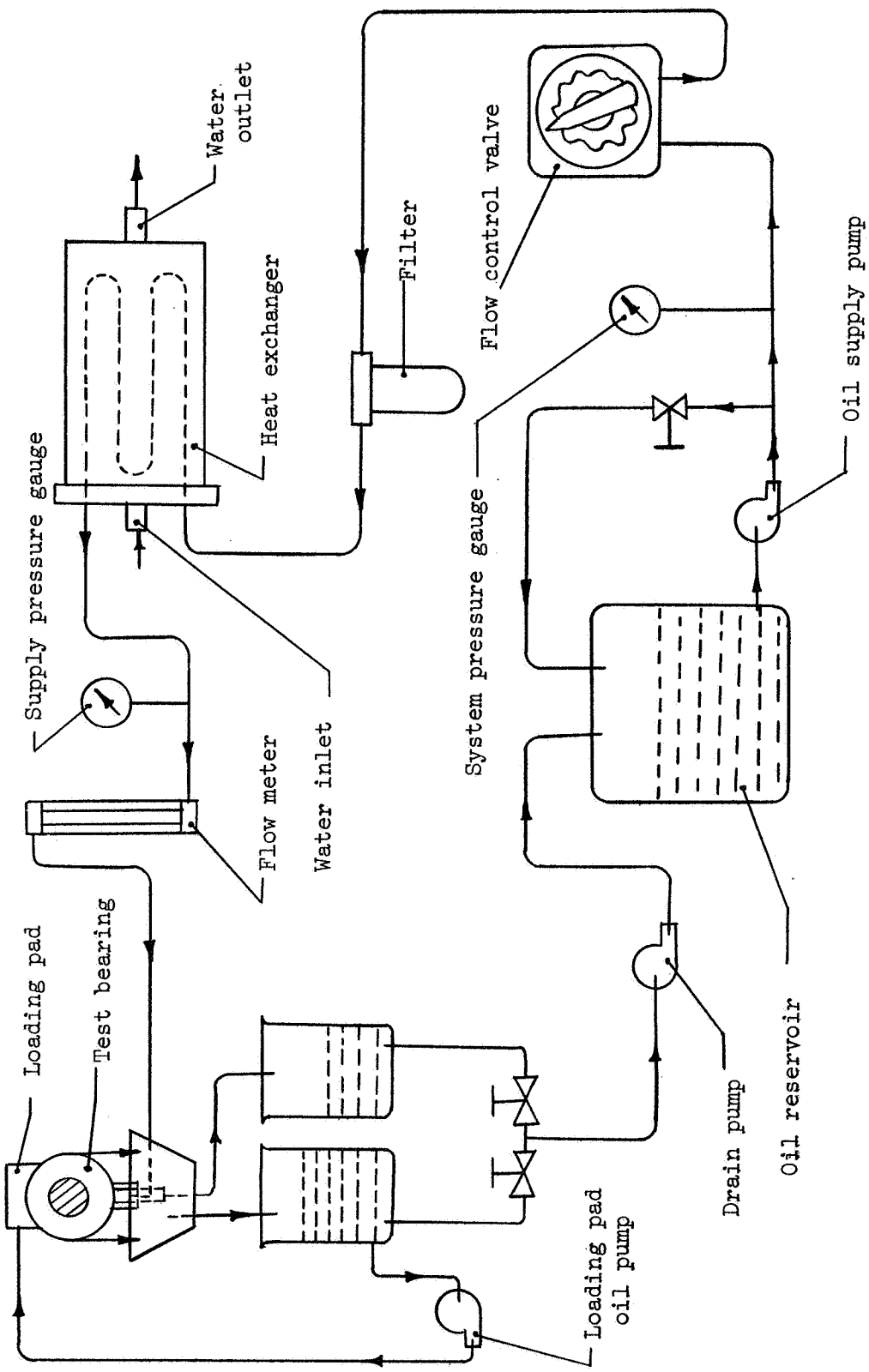

Figure 5. Hydraulic system schematic.

eccentricity under dynamic conditions. The device, which consists of a sensing element and a detector driver, operates on inductive proximity principles. The detector driver provides the energy for the sensing element, and it incorporates an adjustment that may be used to vary sensitivity, providing a wide choice of scale factors. The device requires an external regulated power supply that will deliver 18 volts dc at 20 ma. The output of the detector driver is a negative dc voltage that varies from 0 to 16 volts. The output varies linearly with the clearnace between the conductive surface and the sensing element. Figure 6 illustrates a schematic diagram for the installation of the device. The actual film thickness was determined by subtracting the change in clearance caused by the thermal expansion of the bearing from the film thickness determined from the voltage output of the detector driver. The calibration of the device is described in Appendix B.

III. FRICTION TORQUE MEASUREMENT

A thin cantilever beam as shown in Figure 7 was used to measure the torsional constraint. The friction torque exerted by the bearing was transmitted through the torque arm to the torque beam. Four resistance type strain gages were attached to the torque beam to indicate the strain on the strain indicator. The calibration of the torque beam is described in Appendix C.

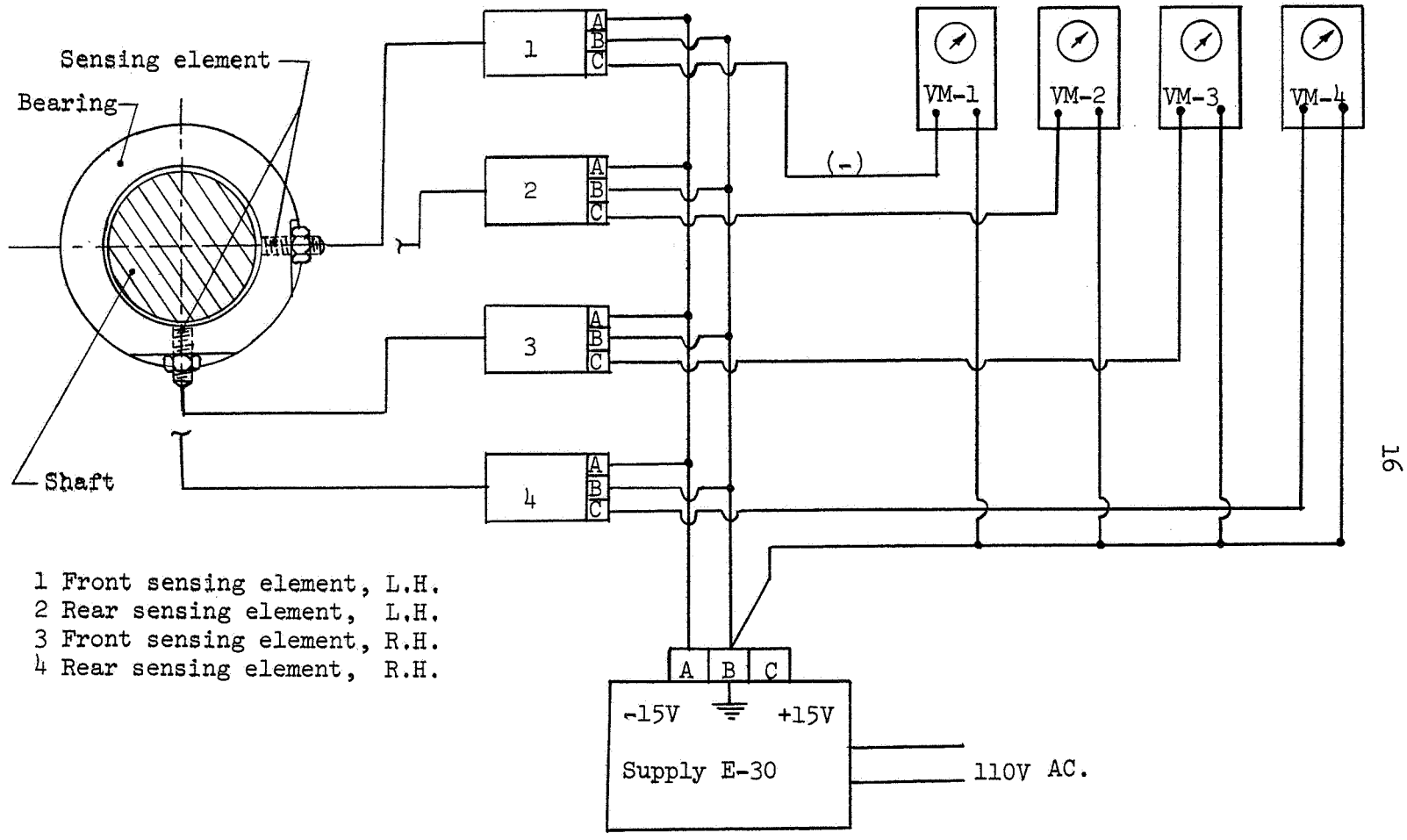

Figure 6. Eccentricity measuring system schematic.

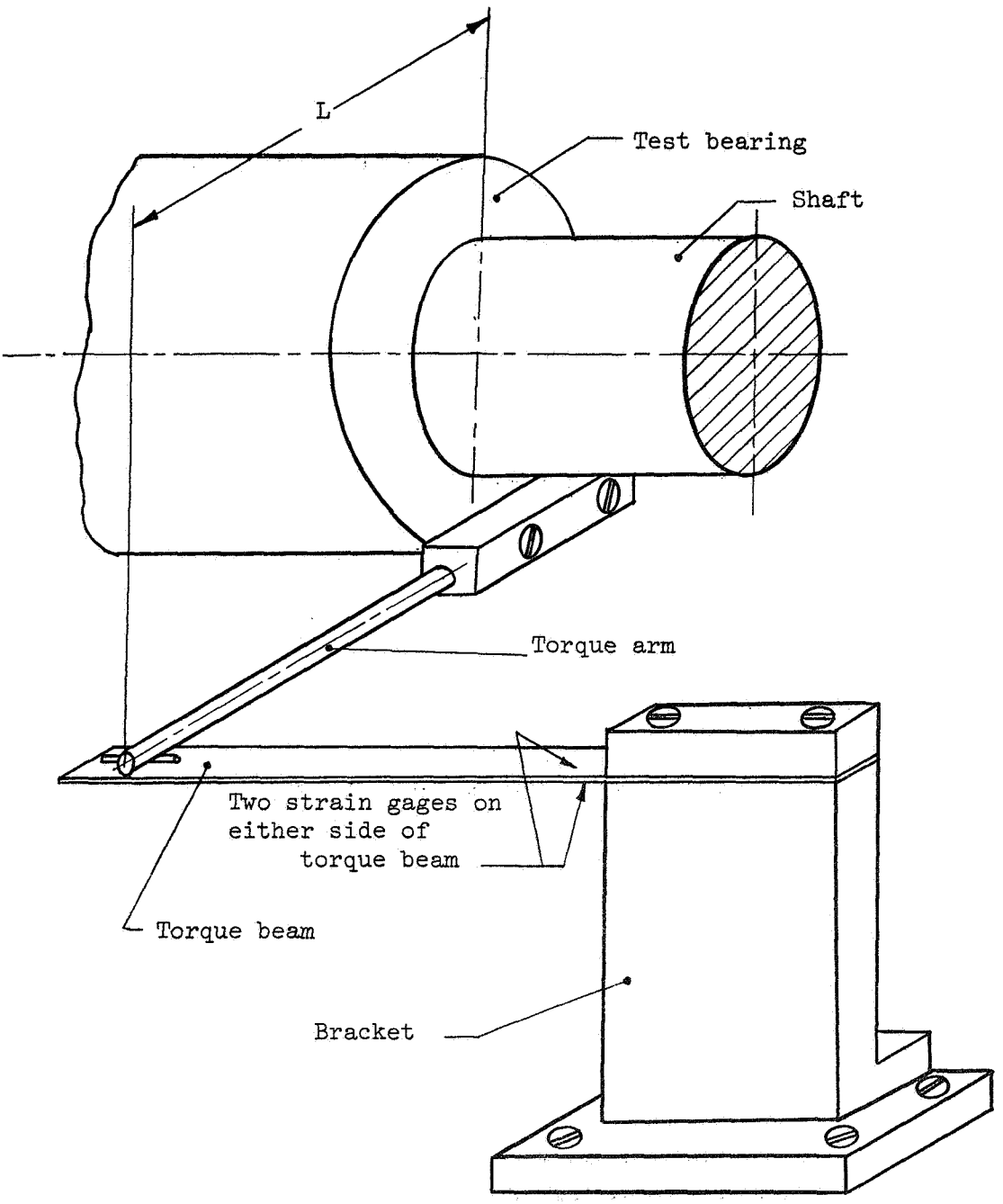

Figure 7. Torque-beam assembly.

IV. TEMPERATURE MEASUREMENT

Two thermocouples were inserted in the bearing drain pipes to measure the oil exit temperature. One thermocouple was located in the oil inlet tube immediately after the flow meter. Copper-constantan thermocouples were connected to a Rubicon Potentiometer, and the reference junction was kept in an ice bath. The oil exit temperature was taken as the film temperature in the bearing, and viscosities based on these temperatures were used in the calculation of the bearing performance. An equation was derived by the series solution method to calculate the oil temperature for any voltage. This equation was:

$$T = -1.094V^2 + 47.42V + 30.48 \ , \qquad (23)$$

wherein V is the potentiometer voltage in millivolts and T is the temperature in degrees Fahrenheit. The difference between the calculated value of T and the value supplied by the manufacturer of the thermocouple was found to be less than 0.5 per cent.

V. OIL FLOW MEASUREMENT

A Fischer and Porter tri-flat flow meter was used to measure the flow rate of the lubricating oil entering the bearing. The flow meter was calibrated so that the flow rate could be available at any given supply oil temperature and float indication. Two methods were available by which the flow meter calibration could be achieved. The first

employs actual measurements of the flow rates at different temperatures and scale readings. The second method employs theoretical principles predicting the meter calibration. In the first method, the constant temperature during the flow rate measurement was not guaranteed. Therefore, the second method outlined by Fischer and Porter [8] was employed in calibrating the flow meter. The complete calibration solution was obtained by running the program on the IBM 7040 computer. This calibration gave the flow rates for temperatures ranging between 66.6° F and 90° F in increments of 0.1° F , and for scale readings of 1 to 25 with an increment of 1. The calibration of the flow meter is described in Appendix D. Several flow rates were actually measured and compared with the theoretical predictions for the same temperatures and scale readings. The difference between predicted and actual value was found to be less than 6 per cent.

VI. PROPERTIES OF GULF HARMONY 47 OIL

Oil viscosities in Saybolt Universal Seconds at any temperature within the operating range can be obtained from Figure 8. The conversion from SUV seconds to centipoises can be obtained by:

$$Cp = (0.22t - 180/t)\ \rho . \tag{24}$$

where t is the viscosity in SUV seconds. The viscosity in Reyns or lb_f-sec/inch^2 is obtained by:

$$\mu = (1.45 \times 10^{-7})\ Cp \ . \tag{25}$$

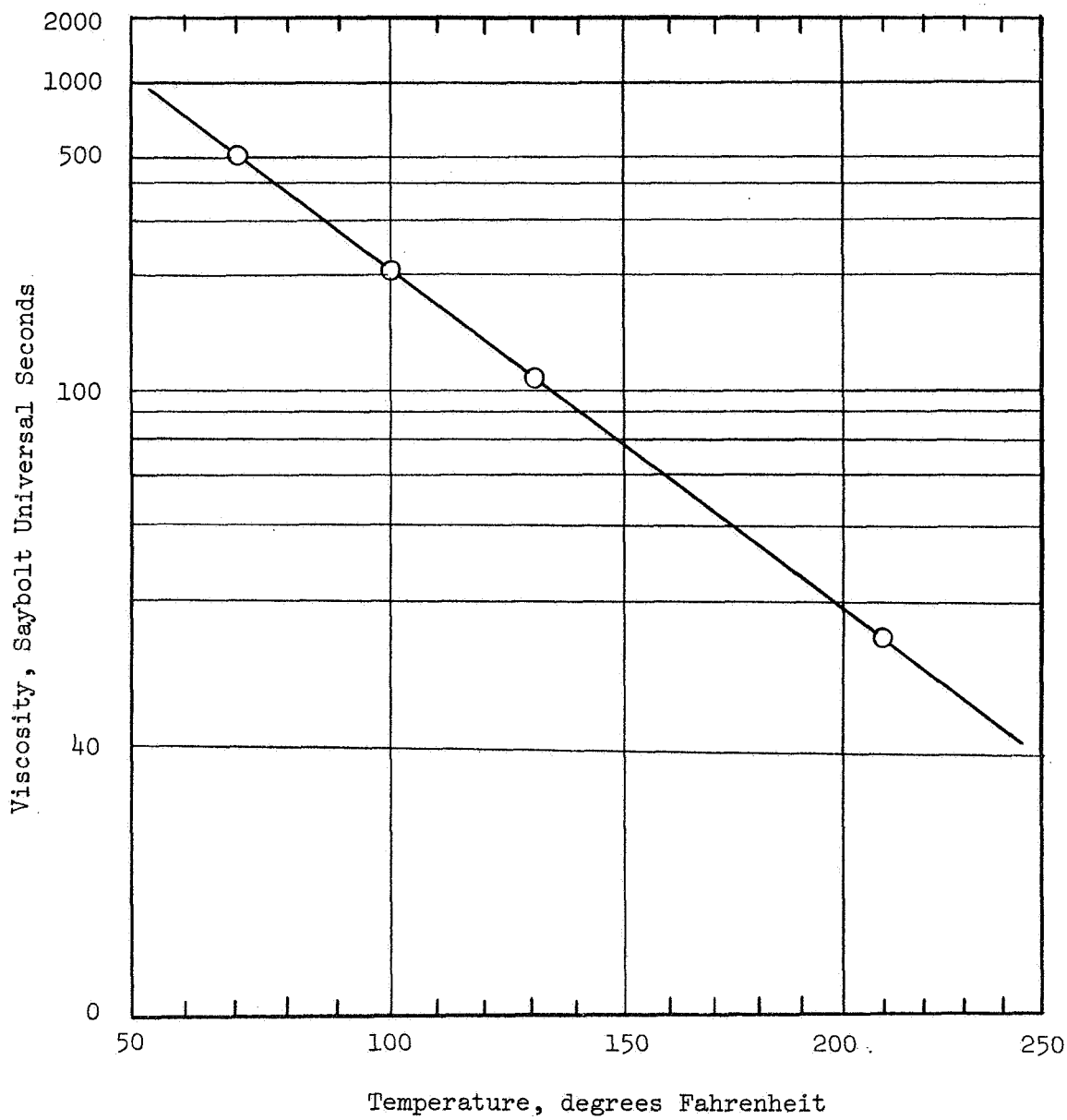

Figure 8. Viscosity versus temperature on ASTM type B chart.

However, for convenience in the use of the computer, the Lagrangian interpolation method was employed. This method would give the viscosity in Reyns or centipoises at any temperature for four degrees of interpolation. The error involved in this method was estimated to be approximately 1 per cent.

The relation between temperature and density [9] was obtained as:

$$\rho = 0.873 - (T-60)(3.43 \times 10^{-4}) \ . \qquad (26)$$

VII. TEST PROCEDURE

In this study, nineteen test series were conducted on Bearing No. 1 and fourteen test series were conducted on Bearing No. 2. Tables I and II illustrate the nature of each test for Bearings No. 1 and No. 2 respectively. The manner in which the data were recorded is shown in Table VII, Appendix A. Before beginning a test, a 30-minute period of running the equipment at constant speed was allowed so that the system would tend toward thermal equilibrium.

TABLE I

DETAILS OF TEST SERIES ON BEARING NO. 1

Test Series No.	Load	Speed	Flow Rate	Other
1	constant	constant	varied	*
2	varied	varied	constant	
3	constant	constant	varied	*
4	varied	varied	constant	
5	constant	varied	constant	
6	constant	varied	constant	
7	varied	varied	constant	
8	varied	constant	constant	
11	varied	varied	constant	
12	varied	varied	constant	
13	varied	varied	constant	
14	varied	constant	constant	
15	varied	varied	constant	
16	varied	varied	constant	
17	varied	varied	constant	
18	constant	varied	constant	
19	constant	varied	constant	
20	constant	varied	constant	
21	constant	varied	constant	

*The bearing supply pressure was adjusted to pre-selected value.

TABLE II

DETAILS OF TEST SERIES ON BEARING NO. 2

Test Series No.	Load	Speed	Flow Rate	Other
22	varied	varied	constant	
23	varied	varied	constant	
24	constant	constant	varied	*
25	constant	constant	varied	*
26	constant	constant	varied	*
27	constant	constant	varied	*
28	constant	constant	varied	*
29	constant	constant	varied	*
30	constant	constant	varied	*
31	constant	constant	varied	*
32	constant	constant	varied	*
33	constant	constant	varied	*
34	constant	constant	varied	*
35	constant	constant	varied	*

*The bearing supply pressure was adjusted to pre-selected value.

CHAPTER III

RESULTS ON BEARINGS NO. 1 AND NO. 2

The effect of the bearing supply pressure on the bearing eccentricity ratio was studied in two different ways. In the first method, test series 1 and 3 were conducted at constant load and constand speed. Variation in the bearing supply pressure was achieved by altering the oil flow rate. The plot of the bearing eccentricity ratio versus the bearing supply pressure is shown in Figure 9. In the second method, a change in the bearing supply pressure was effected by changing the bearing eccentricity ratio, which in turn was altered by varying the load and speed. Figure 10 indicates the relationship between the bearing supply pressure and the bearing eccentricity ratio.

Figure 11 compares the theoretical shaft center locus with the experimentally measured values. The theoretical values of attitude angle, based on the Short-bearing Approximation, were obtained from Equation (20). The experimental values of the attitude angle were obtained from Equation (53). This indicated that the viscoseal bearing operates at high eccentricity ratio even at high attitude angle.

Figure 12 compares the theoretical capacity number with the experimentally measured values. The experimental and theoretical values of the capacity number,based on the Short-bearing Approximation,were obtained from Equation (19).

Friction characteristics of the bearing are presented in Figures 13 and 14. The experimental and theoretical values of friction ratio,

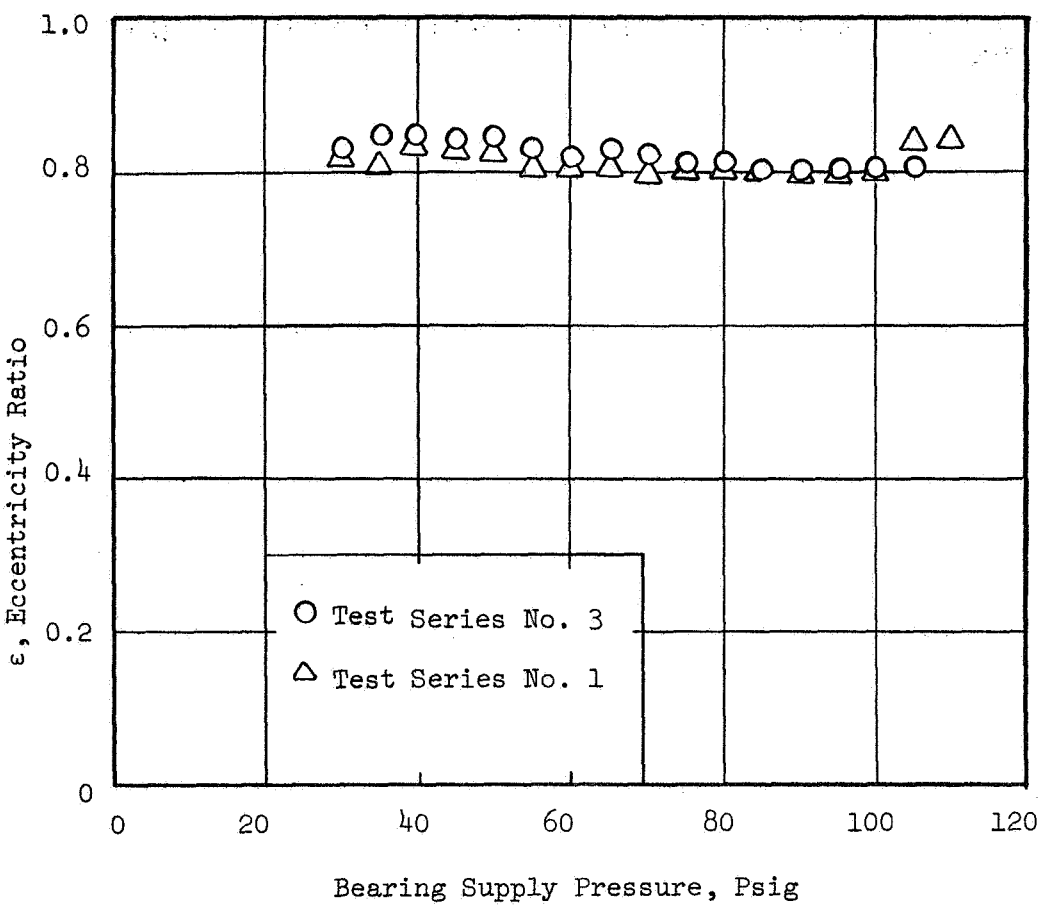

Figure 9. Bearing supply pressure versus eccentricity ratio at constant load and constant speed.

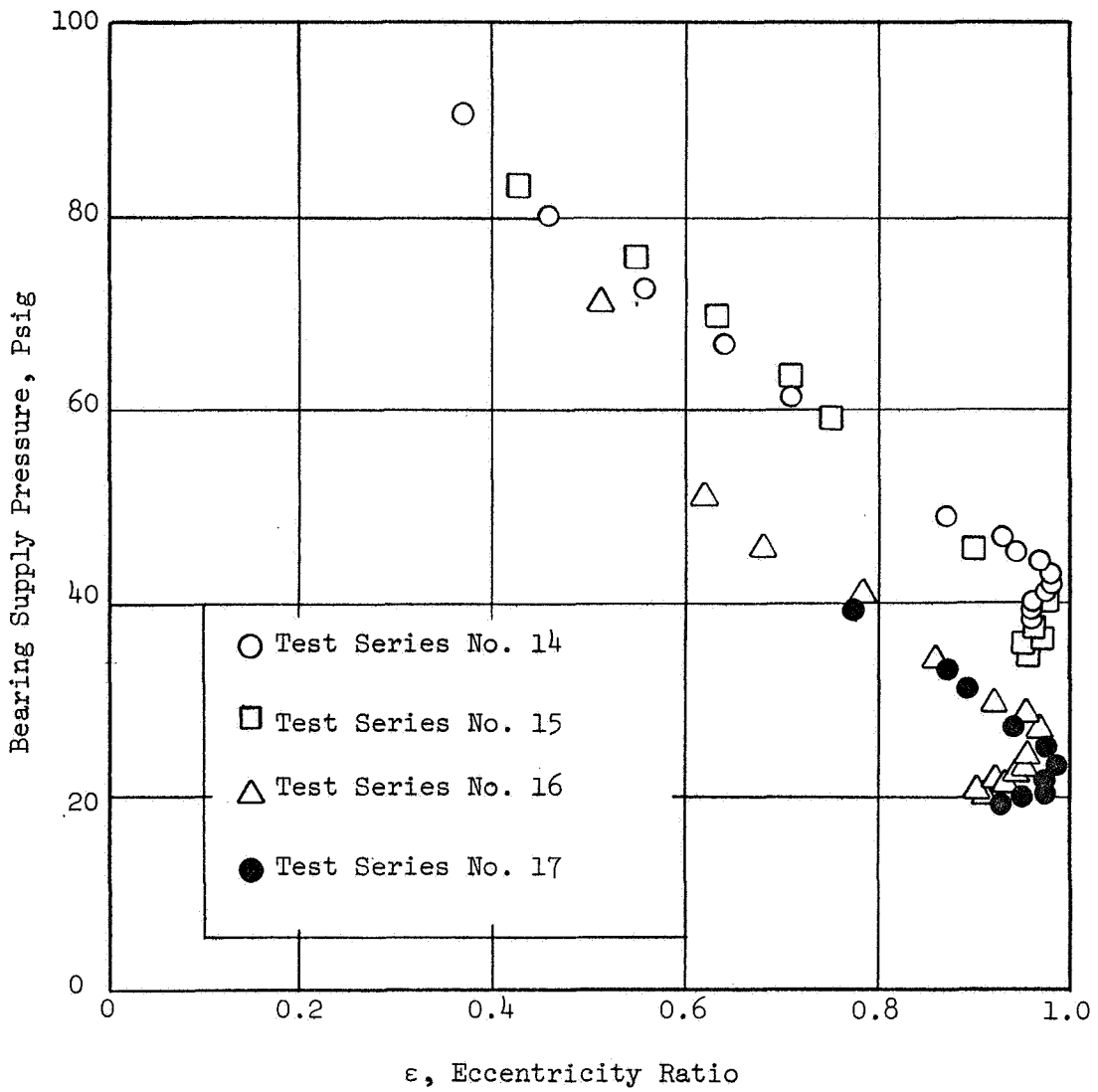

Figure 10. Bearing supply pressure versus eccentricity ratio at constant flow rate.

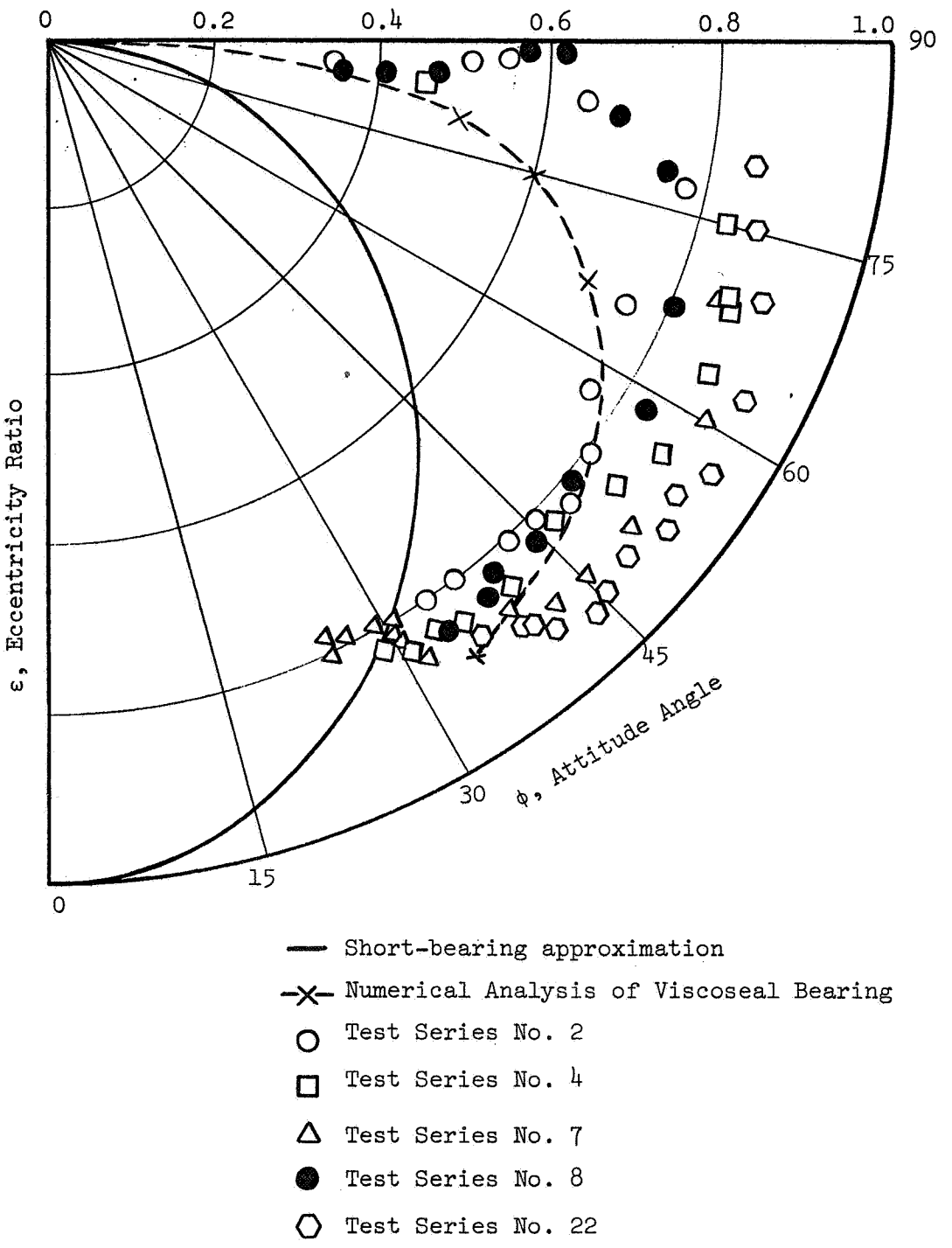

Figure 11. Eccentricity ratio versus attitude angle.

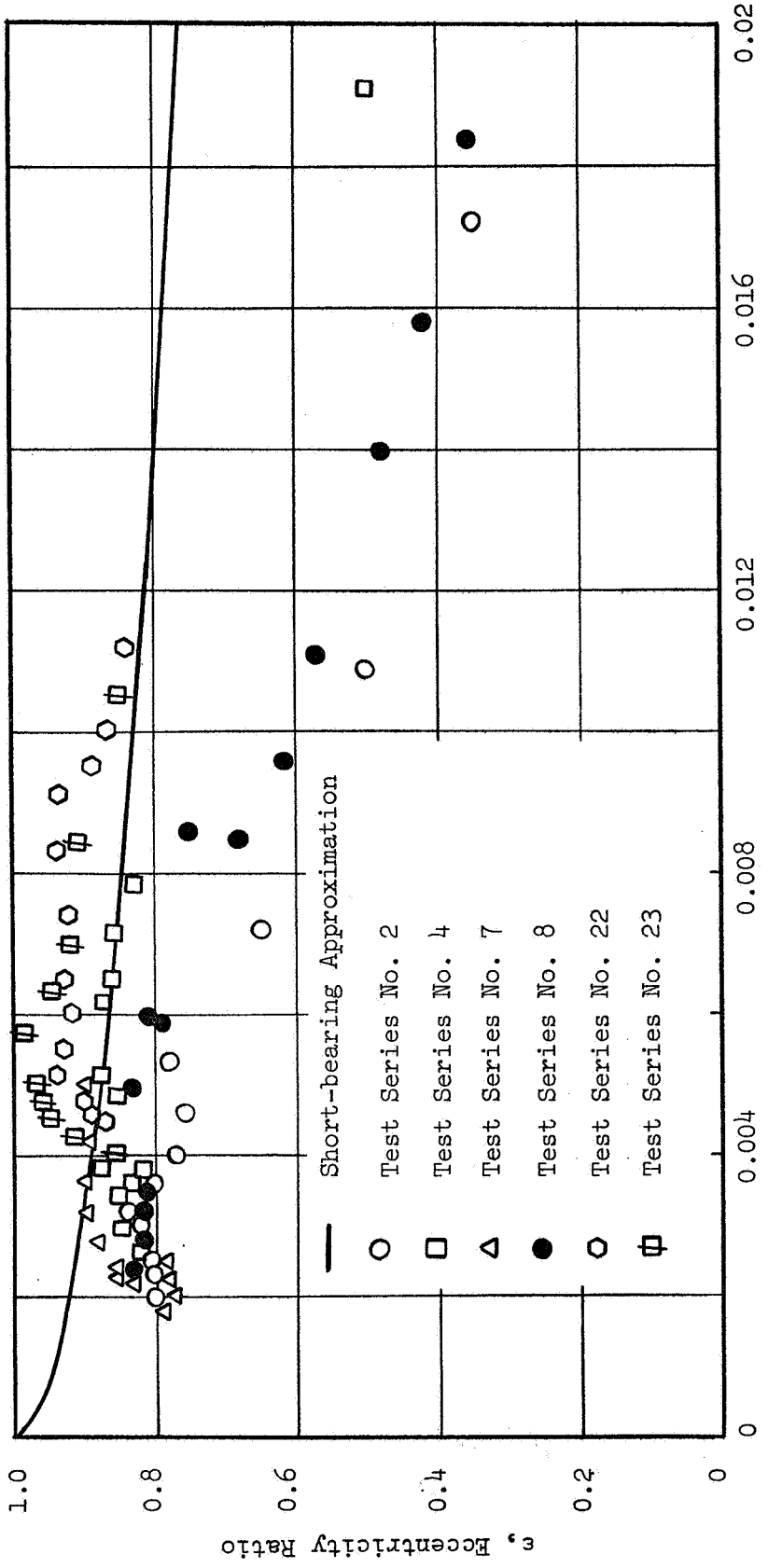

Figure 12. Capacity number versus eccentricity ratio.

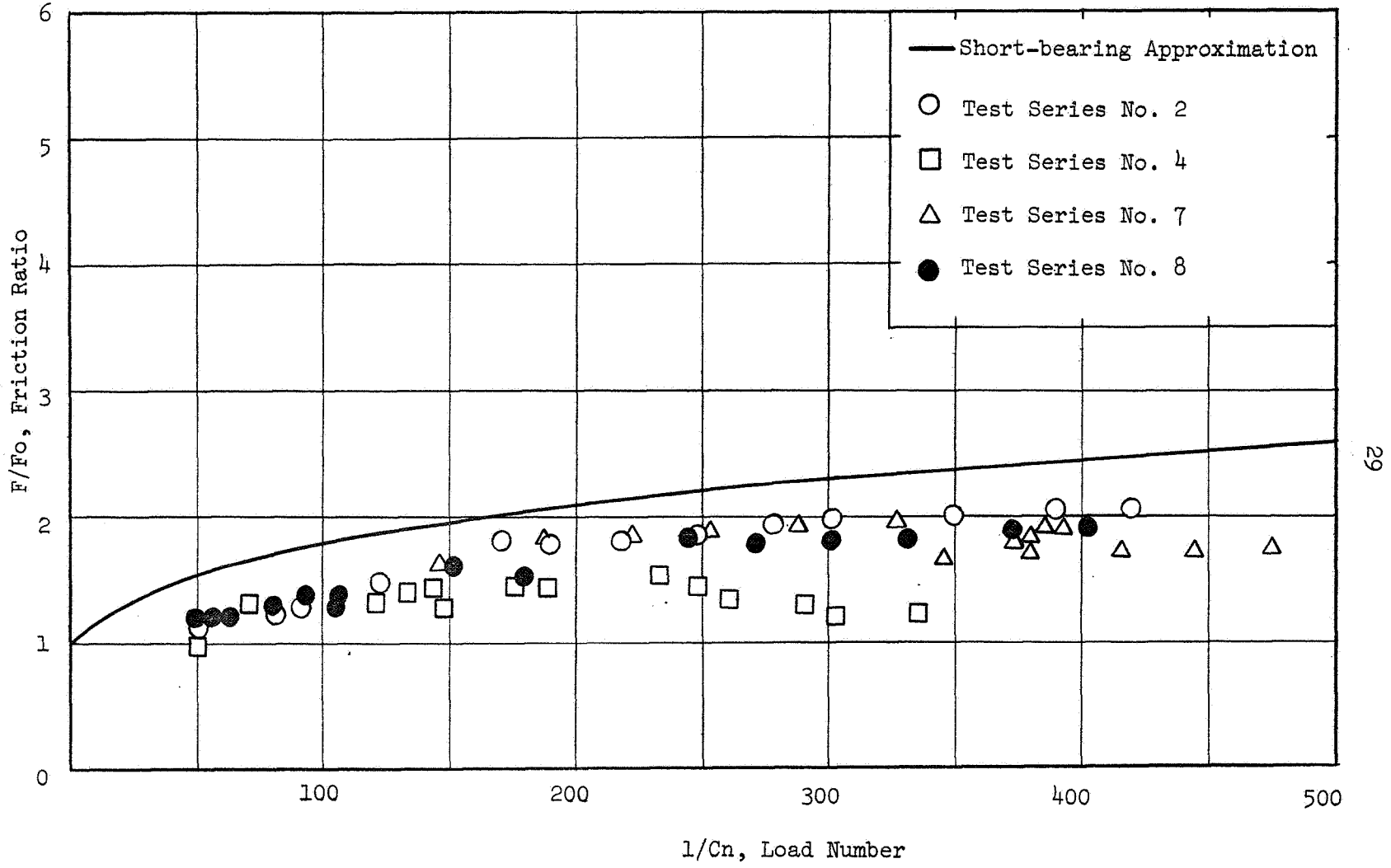

Figure 13. Load number versus friction ratio.

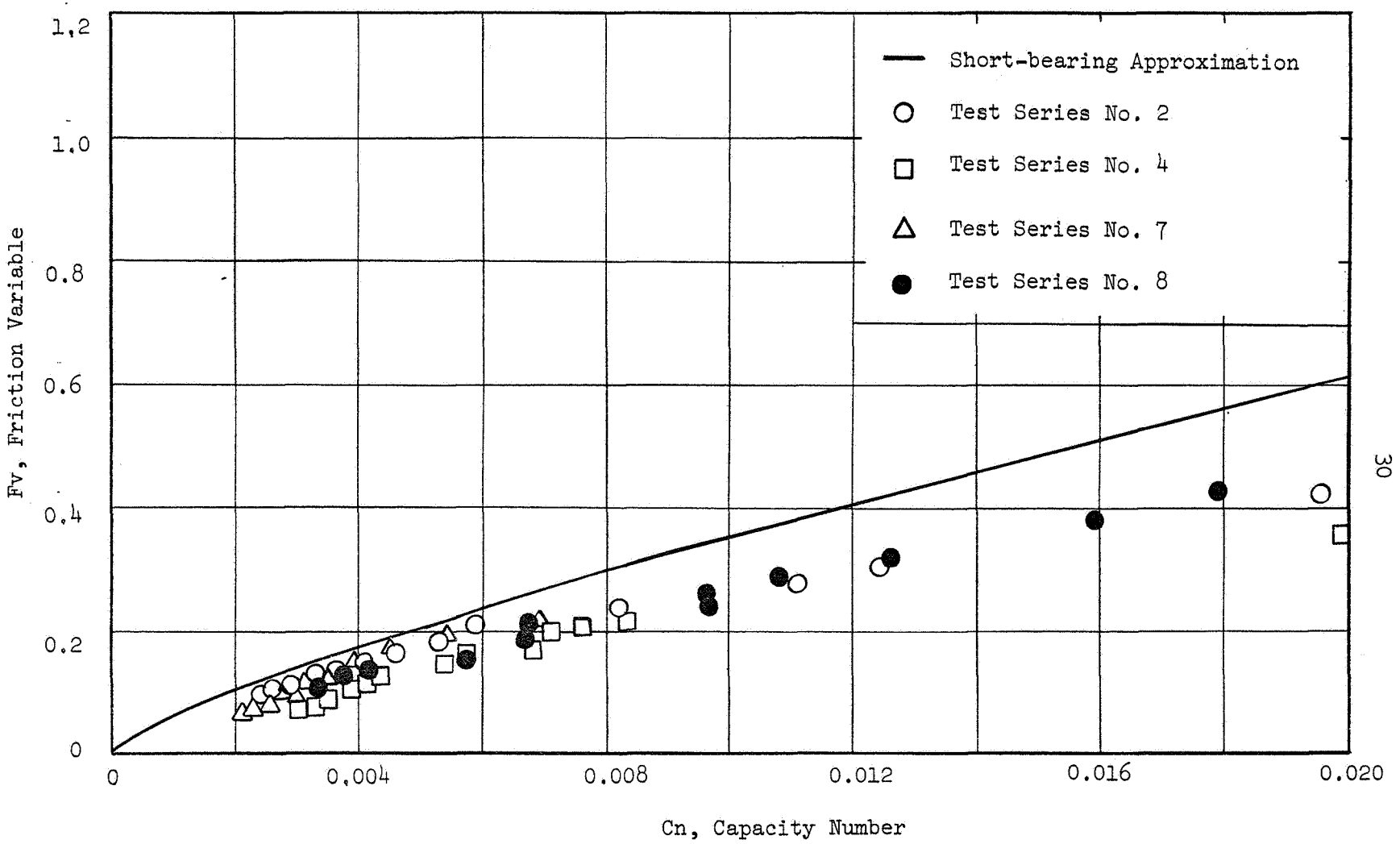

Figure 14. Capacity number versus friction variable.

F/Fo , and friction variable, Fv , were obtained from Equations (21) and (22).

Figure 12, page 28, also illustrates the performance of Bearing No. 2 having a wider land. From this figure, for 0.85 eccentricity ratio, the approximate capacity numbers for Bearings No. 1 and No. 2 were found to be 0.0025 and 0.0055 respectively. Thus, the ratio of capacity number of Bearing No. 2 to that of Bearing No. 1 is:

$$\frac{Cn_{VB,E,2}}{Cn_{VB,E,1}} = \frac{0.0055}{0.0025}$$

$$= 2.2 \ . \qquad (27)$$

From Equation (18), for the same eccentricity ratio, surface velocity, and viscosity, the ratio of the theoretical load-carrying capacities of the two bearings is:

$$\frac{W_{VB,T,2}}{W_{VB,T,1}} = (a_2^3/c_2^2)/(a_1^3/c_1^2)$$

$$= (0.233/0.1667)^3(0.0026/0.0025)^2$$

$$= 2.94. \qquad (28)$$

The percentage of load-carrying capacity of the viscoseal bearing was computed in two different ways. For example, in test series No. 7, the experimental eccentricity ratio was found to be 0.862 for a total load of 70.6 lb. For the same eccentricity ratio, the theoretical load-

carrying capacity of the viscoseal bearing having eight grooves was computed from Equation (18):

$$W_{VB,T,1} = \frac{8\mu\, Ua^3}{4c^2} \frac{\varepsilon}{(1-\varepsilon^2)^2} \left[\pi^2 (1 - \varepsilon^2) + 16\varepsilon^2\right]^{1/2} . \qquad (29)$$

Thus, under identical conditions, the percentage of experimental load-carrying capacity to the theoretical one is:

$$\frac{W_{VB,E,1}}{W_{VB,T,1}} 100 = 98.31 \text{ per cent} . \qquad (30)$$

The theoretical load-carrying capacity of the plain journal bearing of the same overall dimensions computed from Equation (18) is:

$$W_{JB,T,1} = \frac{2\mu\, U\ell^3}{4c^2} \frac{\varepsilon}{(1-\varepsilon^2)^2} \left[\pi^2 (1 - \varepsilon^2) + 16\varepsilon^2\right]^{1/2} . \qquad (31)$$

Thus, the percentage of experimental load-carrying capacity of the viscoseal bearing to the theoretical load-carrying capacity of the plain journal bearing of the same overall dimensions may be found by:

$$\frac{W_{VB,E,1}}{W_{JB,T,1}} 100 = 0.70 \text{ per cent.} \qquad (32)$$

Tables III and IV show such comparison for test series No. 7 for Bearing No. 1 and Test series No. 22 for Bearing No. 2 respectively.

TABLE III

PERCENTAGE LOAD-CARRYING CAPACITY OF BEARING NO. 1[a]

Eccentricity Ratio	$\frac{(W_{VB,E,1})(100)}{(W_{VB,T,1})}$	$\frac{(W_{VB,E,1})(100)}{(W_{JB,T,1})}$
0.8623	98.31	0.700
0.8952	73.99	0.527
0.8980	81.96	0.584
0.8973	97.09	0.692
0.8944	117.80	0.839
0.8717	201.44	1.436
0.8530	299.60	2.135
0.8466	348.19	2.482
0.8290	449.43	3.203
0.8202	485.26	3.459
0.8217	470.34	3.352
0.7947	585.78	4.175
0.7908	678.66	4.837
0.7818	809.09	5.767
0.7745	930.12	6.629
0.7959	806.84	5.751

[a]Test Series No. 7.

TABLE IV

PERCENTAGE LOAD-CARRYING CAPACITY OF BEARING NO. 2[a]

Eccentricity Ratio	$\frac{(W_{VB,E,2})(100)}{(W_{VB,T,2})}$	$\frac{(W_{VB,E,2})(100)}{(W_{JB,T,2})}$
0.8434	68.83	1.783
0.8691	53.12	1.376
0.8913	38.09	0.987
0.9342	14.41	0.373
0.9386	13.73	0.356
0.9225	24.76	0.641
0.9331	20.80	0.539
0.9178	34.81	0.902
0.9318	25.65	0.664
0.9362	23.94	0.620
0.9219	38.43	0.996
0.8967	68.90	1.785
0.8854	89.09	2.308
0.8645	128.59	3.331

[a]Test Series No. 22.

The sealing performance of the bearings was determined in two ways. In the first, the sealing coefficient was computed by substituting the bearing supply pressure for the term Δp in Equation (1). The values obtained from test series Nos. 14, 15, and 18 were compared with the theoretical values obtained from Equations (2) through (12), as shown in Figure 15. In the second method, test series nos. 25 through 35 were conducted at constant load, constant speed, and varying flow rates. The term Δp in Equation (1) was taken as the bearing supply pressure. Graphs of $\Delta p/\mu$ versus flow rate were plotted for each test series. Figure 16 illustrates such a graph for test series No. 25. This curve, essentially a straight line, was extended as shown by a broken line in the figure, to obtain $\Delta p/\mu$ for zero flow rate. Thus, the sealing coefficient was computed by substituting the above value of $\Delta p/\mu$ in Equation (1). The results obtained from test series Nos. 25 through 35 are plotted in Figure 15.

Figure 17 indicates the effect of eccentricity ratio on the sealing coefficient. The theoretical curve was plotted from the analysis performed by Vohr and Chow [6]. The experimental values were obtained by the first method described in the preceding paragraph. Although the experimental values and theoretical predictions are far from agreement, both indicate that the sealing performance deteriorates with an increase in the bearing eccentricity ratio.

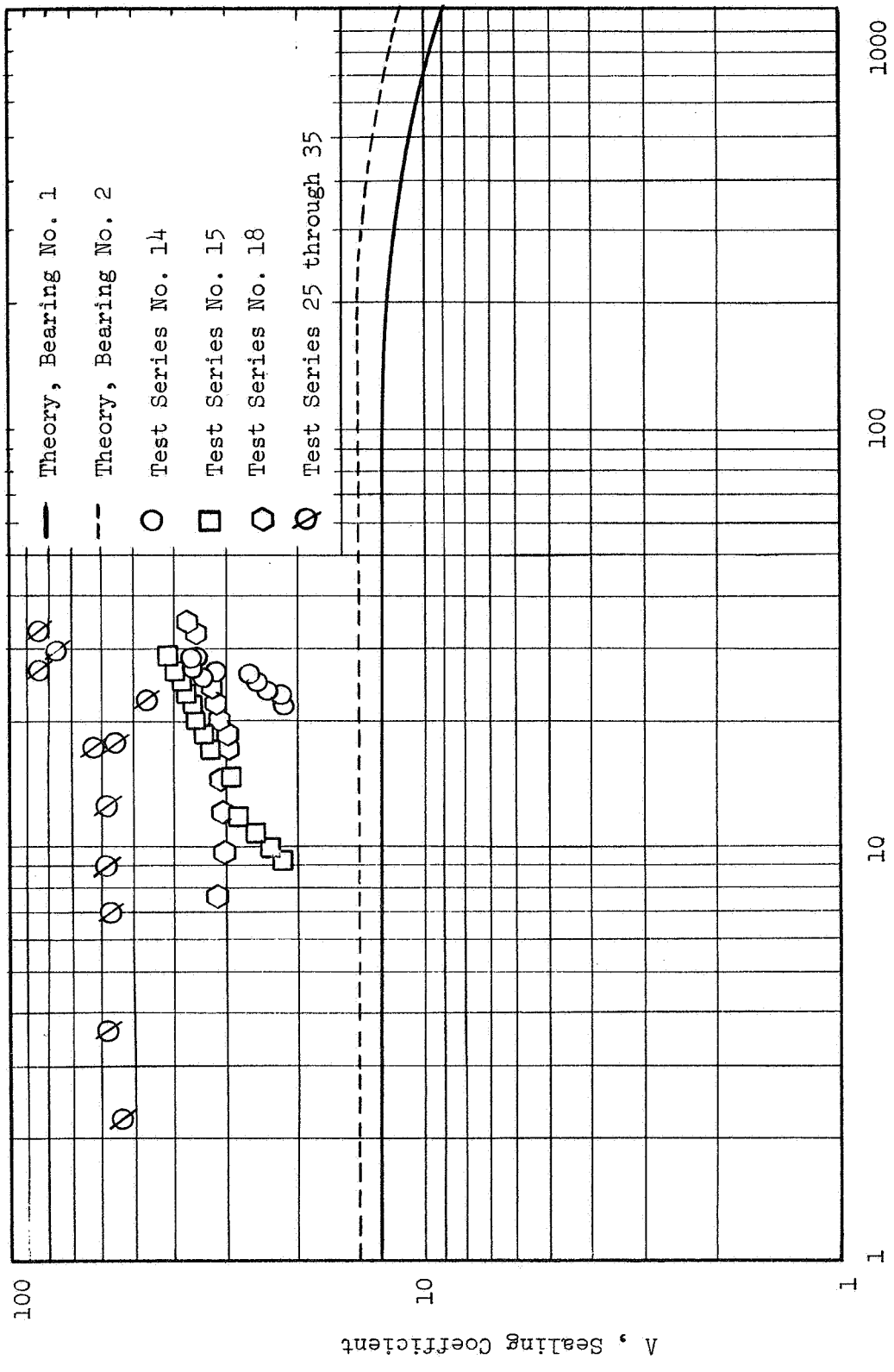

Figure 15. Reynolds number versus sealing coefficient.

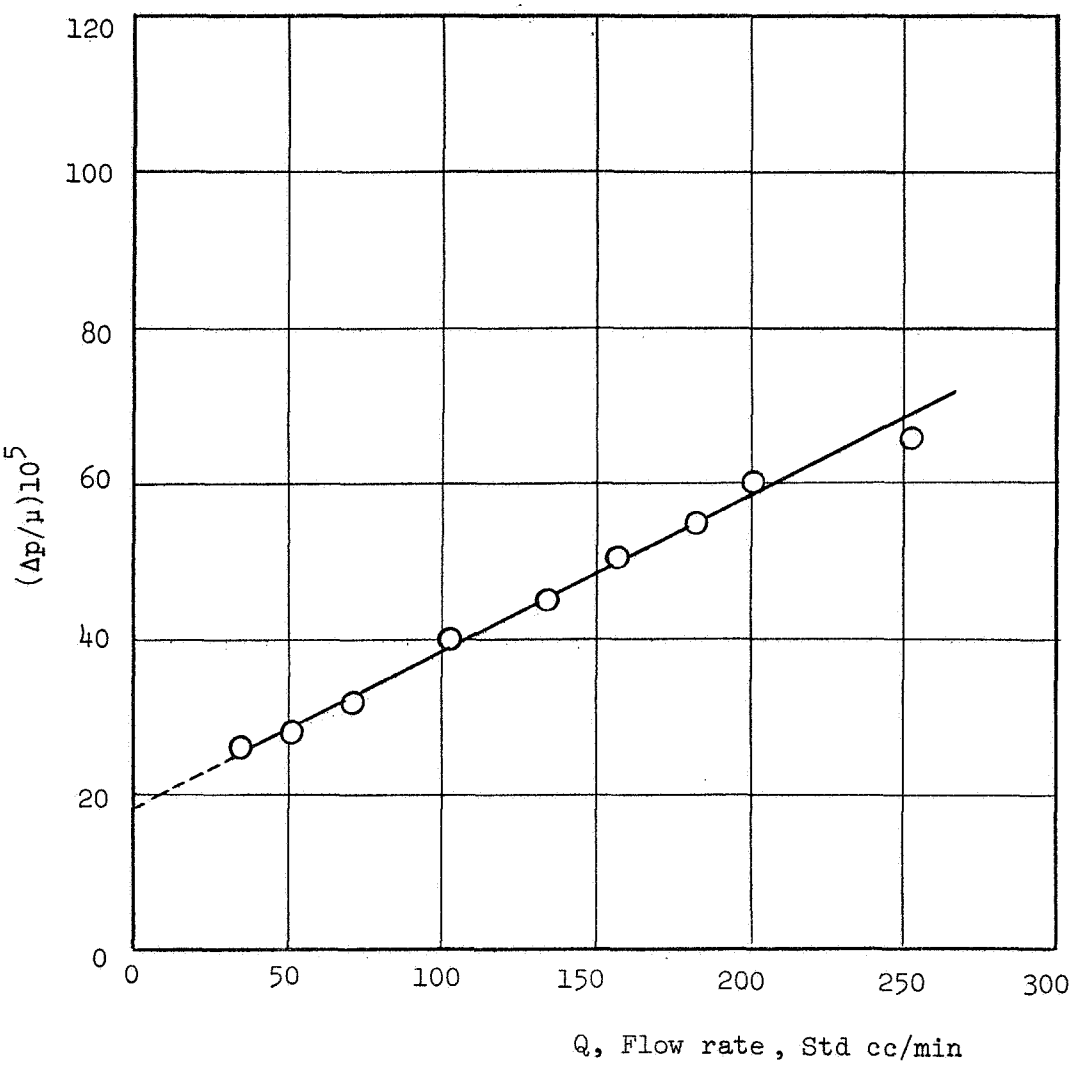

Figure 16. Flow rate versus $\Delta p/\mu$.

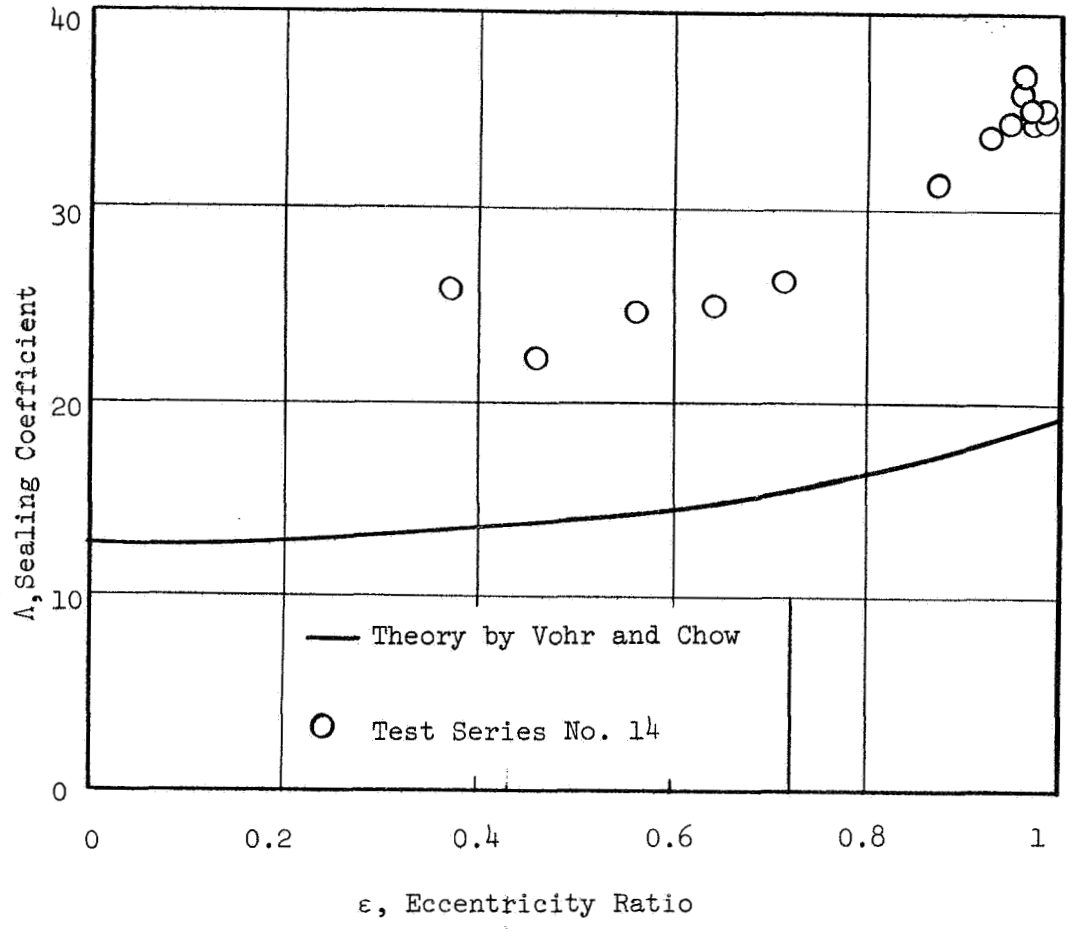

Figure 17. Eccentricity ratio versus sealing coefficient.

CHAPTER IV

DISCUSSION AND CONCLUSIONS

Except for the shaft center locus findings, the results obtained from the experimental study of two different groove geometries of the viscoseal bearing seemed to be in fair agreement with the Short-bearing Approximation. The actual picture obtained from Figure 12, page 28, however, was not very satisfactory. The extent to which the experimental results agreed with the Short-bearing Approximation is indicated in Tables III and IV, pages 33 and 34. It is interesting to note, however, from available data of the work by Dubois and Ocvirk [7], that their experimental results also did not agree very well with their own theoretical analysis. This information is presented in Table V.

The locus of shaft center is an important parameter in bearing performance. The experimental evidence indicated that the bearing operated at high eccentricity ratio even at high attitude angle. The nature of the curve, as shown in Figure 11, page 27, indicated that the behavior was similar to that of a gas bearing or an elliptical bearing. Shaw and Macks [10] have pointed out that in the loaded area of the bearing, the grooves tend to disrupt the formation of high fluid pressure. Radzimovsky [11] describes the influence of circumferential groove on pressure distribution as shown in Figure 18, from which it is clear that the total load-carrying capacity of two short bearings each of length l' is much smaller than that of the bearing having

TABLE V

THEORETICAL AND EXPERIMENTAL CAPACITY NUMBER FOR A PLAIN JOURNAL BEARING BY DUBOIS AND OCVIRK[a]

Eccentricity Ratio	Short-bearing Approximation for Capacity Number		Ratio of Experimental Cn to Theoretical Cn
	Theoretical	Experimental	
0.253	0.8238	0.5200	0.63
0.384	0.1835	0.2880	1.57
0.477	0.1186	0.2000	1.69
0.531	0.0907	0.1530	1.69
0.623	0.0546	0.1030	1.89
0.695	0.0341	0.0772	2.26
0.740	0.0242	0.0621	2.57
0.805	0.0131	0.0445	3.30
0.860	0.0066	0.0347	5.25
0.897	0.0035	0.0279	7.92

[a] $l/d = 1/2$, Supply Pressure = 100 $lb/inch^2$.

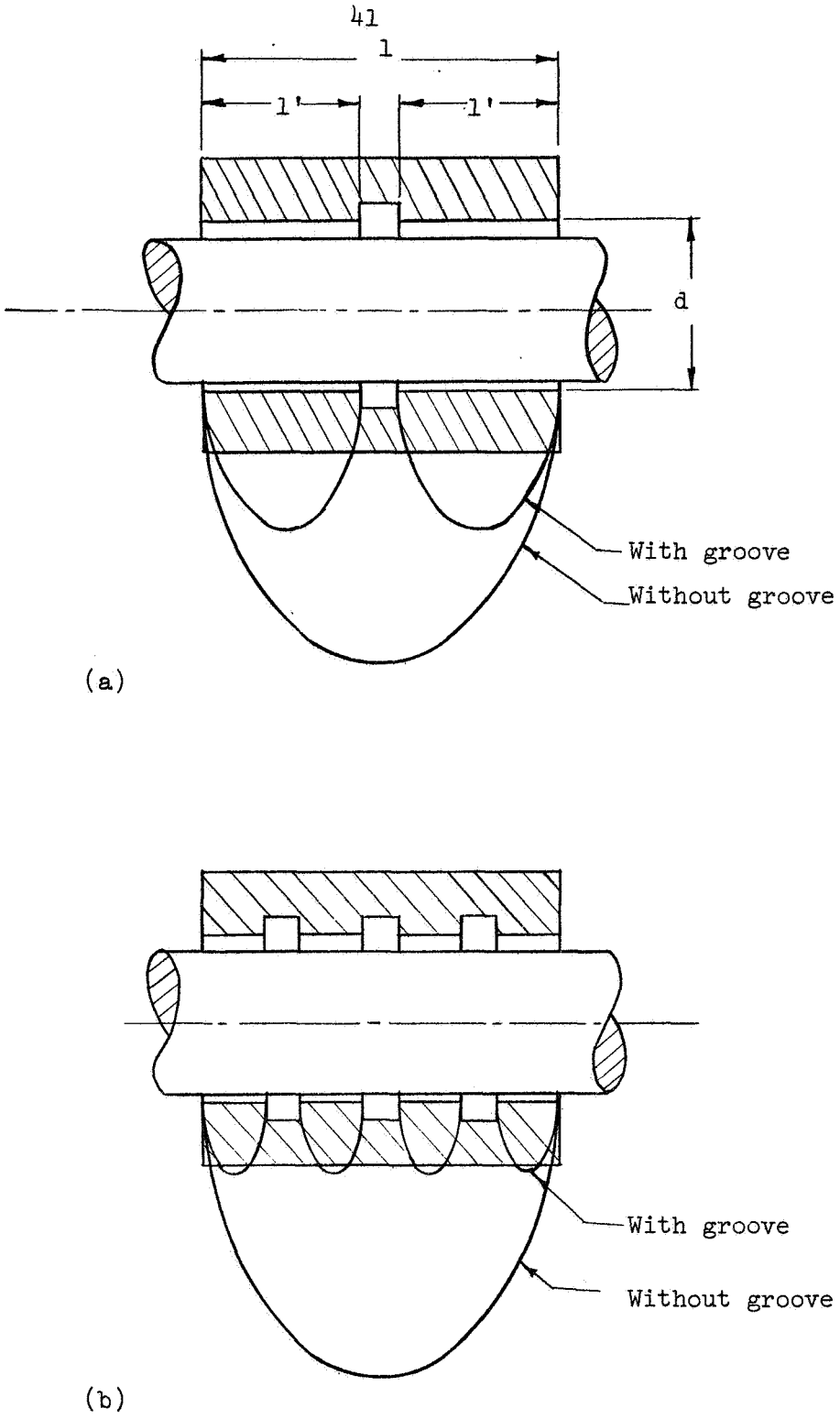

Figure 18. Influence of a circumferential groove upon the axial pressure distribution in the oil film. (a) Bearing with one groove; (b) bearing with three grooves.

length l. Therefore, the bearing having a circumferential groove will have a greater eccentricity ratio than a comparable bearing without such a groove operating under identical conditions. Or, in other words, for a given oil-film thickness, the load is smaller than a permissible load for a bearing without circumferential groove, but with other operating conditions and bearing characteristics being identical. The effect becomes more pronounced, as the number of grooves increases, as shown in Figure 18b, page 41.

Very interesting but limited data were available from W. L. Roberts [12], who is presently engaged in investigating the numerical computation of the load capacity and stability of the viscoseal bearing under a project entitled "An Analysis of the Viscoseal Bearing." Shaft center locus obtained from these data seemed to agree better than the Short-bearing Approximation as shown in Figure 11, page 27. The loads computed from the numerical analysis were compared with the experimental values in Table VI. From these data it is evident that the numerical analysis agrees well with the experimental results.

From Figure 12, page 28, it will be observed that the experimental results obtained from Bearing No. 1 are of a different nature than those obtained from Bearing No. 2 in that the values of eccentricity ratio for Bearing No. 2 lie farther above the theoretical curve than those for Bearing No. 1. The drain pipes fitted to the drain tubes of Bearing No. 1 seemed to prevent the free movement of the bearing, and they were removed during the test runs for Bearing No. 2. This modification may

TABLE VI

EXPERIMENTAL AND THEORETICAL LOAD-CARRYING CAPACITIES OF BEARING NO. 1[a]

Eccentricity Ratio	Experimental Load, Lb.	Load Computed by Numerical Analysis of Complete Reynolds Equation, Lb.	Load Computed by Short-bearing Approximation, Lb.
0.4697	34.38	33	5.06
0.6036	43.40	36	8.95
0.7226	56.10	44	19.40
0.8347	77.80	75	56.14
0.9000	172.10	158	199.00

[a]Test Series No. 8.

have been the reason for obtaining such results. It may also be observed from Figure 12, page 28, that some experimental values of the eccentricity ratios at high capacity numbers were far below the theoretical curve. The accuracy of these results cannot be guaranteed since Bearing No. 1 vibrated at any load less than approximately 50 lb. and at a speed of approximately 2000 RPM. For Bearing No. 2, vibration occurred at a load of approximately 100 lb. and a speed of 1500 RPM. This vibration caused difficulty in or prevented the obtaining of readings on the film thickness measurement device.

Very careful observation of Figures 10, 11, and 12, pages 25, 26, and 27 reveals that after a certain point the bearing eccentricity ratio decreased slightly with an increase in load.

The sealing performance of the bearings, determined by two different methods, did not agree with the theoretical predictions. This may indicate the need for a different approach to the determination of the sealing coefficient. It should be noted that the bearing always has some flow of oil which is opposite to the direction of pumping, as shown in Figure 2, page 7. Thus, the bearing functions neither as a viscoseal nor as a viscopump. Therefore, it is suggested that a three-way valve be incorporated in the oil supply line prior to the supply pressure gauge so that during an experiment the oil supply to the bearing may be cut off momentarily by the valve and the resulting pressure noted. Presumably this pressure would be the pressure generated by the viscoseal bearing, and when substituted for Δp in Equation (1) would give the correct sealing coefficient.

Finally the following conclusions were drawn from the study:

1. The eccentricity ratio is not affected by the bearing supply pressure or the flow rate at constant load and speed.

2. The bearing supply pressure decreases with an increase in the bearing eccentricity ratio at a constant flow rate.

3. The shaft center locus of the viscoseal bearing does not follow the Short-bearing Approximation. In fact, the bearing operates at high eccentricity ratio even at high attitude angle.

4. The experimental results were only in fair agreement with the Short-bearing Approximation. However, the agreement found in this experiment was similar to the agreement between theory and experiment found by Dubois and Ocvirk [7].

5. Increasing the land width increases the load-carrying capacity. The experimentally obtained value showed rather close agreement with the theoretically predicted value.

6. Limited data available from the numerical analysis were encouraging. The results showed better agreement with the experiment than did the Short-bearing Approximation.

7. The sealing performance of the viscoseal bearing could not be reliably determined by the methods followed. The actual pressure gradient generated by viscoseal action might be determined by the method suggested in this chapter.

LIST OF REFERENCES

LIST OF REFERENCES

1. Pearsall, R. H. "The Screw Oil Pump," The Automobile Engineer, 15:145-147, May 1924.

2. Stair, W. K. "Theoretical and Experimental Studies of Visco Type and Buffered Shaft Seals," The University of Tennessee, Report ME-65-587-11, May 1968.

3. Stair, W. K. "Effect of Groove Geometry on Viscoseal Performance," Journal of Engineering for Power, 89:605-614 No. 4, Trans. ASME, Series A, October 1967.

4. Stair, W. K., and Hale, R. H. "Analysis of the Viscoseal Part II, the Concentric Turbulent Case," The University of Tennessee, Report ME-66-587-7, June 1966.

5. Stair, W. K. "Analysis of Viscoseal," The University of Tennessee, Report ME-65-587-2, January 1965.

6. Vohr, John, and Chow, C. "Theoretical Analysis of Spiral-grooved Screw Seal for Turbulent Operation," A paper submitted for the presentation at the fourth international conference on fluid sealing, Philadelphia, Pennsylvania, May 1969.

7. Dubois, George, and Ocvirk, Fred. "Analytical Derivation and Experimental Evaluation of Short-bearing Approximation for Full Journal Bearings," NACA Report 1157, 1953.

8. Fischer and Porter. Tri-flat Variable-area Flowmeters, Handbook 10A9010. Warminster: Fischer and Porter Co., January 1964.

9. Fuller, Dudley D. Theory and Practice of Lubrication for Bearings. New York: John Wiley and Sons, Inc., First Edition.

10. Shaw, M. C. and Macks, F. F. Analysis and Lubrication of Bearings. New York: McGraw-Hill Book Company, 1949.

11. Radzimovsky, E. I. Lubrication of Bearings. New York: The Ronald Press Company, 1959.

12. Roberts, W. L. "An Analysis of the Viscoseal Bearing," Unpublished Master's thesis, The University of Tennessee, Knoxville, 1969.

APPENDIXES

APPENDIX A

SAMPLE CALCULATIONS AND DATA SHEET

Table VII shows a typical data sheet for test series No. 16. The symbols used for all the items of the data sheet were the same as those used in the IBM 7040 computer program. The actual calculations for the first reading of the sample data sheet are given below:

Temperatures in degrees Fahrenheit at left and right oil exit are:

$$\text{TEMPL} = -1.094(\text{VTC1})^2 + 47.42(\text{VTC1}) + 30.48$$
$$= 94.59^{\circ}\text{F.} \tag{33}$$

$$\text{TEMPR} = -1.094(1.434)^2 + 47.42(1.434) + 30.48$$
$$= 96.23^{\circ}\text{F.} \tag{34}$$

Average film temperature is:

$$\text{TEMPAV} = (\text{TEMPL} + \text{TEMPR})/2$$
$$= 94.41^{\circ}\text{F.} \tag{35}$$

Supply inlet temperature is:

$$\text{TEMPS} = -1.094(0.822)^2 + 47.42(0.822) + 30.48$$
$$= 68.72^{\circ}\text{F.} \tag{36}$$

TABLE VII

SAMPLE DATA SHEET[a]

Thermocouple Voltage at Oil Exit, mv.		Distance Detector Output, Volts				External Load, lb.	Strain Indication, Micro-Inches/Inch	Speed	Initial Strain in Beam, Micro-Inches/Inch	Thermocouple Voltage at Supply Inlet, mv.	System Supply Pressure, Psig.	Bearing Supply Pressure, Psig.	Flowmeter Indication
Left	Right	1	2	3	4								
VTC1	VTC2	VDD1	VDD2	VDD3	VDD4	W	E	RPM	STRANI	VTC3	SSP	BSP	FI
1.397	1.434	8.92	9.9	9.6	10.3	0.0	2260	1560	1706	0.822	123	70.5	14
1.497	1.525	9.0	10.2	9.8	10.7	0.5	2280	1720		0.82	108	51.0	14
1.523	1.575	9.0	10.45	9.7	10.8	1.0	2318	1820		0.815	105	45.5	14
1.592	1.63	9.3	10.8	9.6	11.1	1.5	2342	1900		0.815	102	40.5	14
1.682	1.705	9.45	10.95	9.7	11.4	2.0	2350	2010		0.815	98	34.0	14
1.815	1.86	9.95	11.0	10.45	11.4	3.0	2393	2200		0.815	95	29.5	14
1.9	1.937	10.25	10.9	11.15	11.25	4.0	2420	2400		0.81	87	28.5	14
1.945	1.995	10.5	10.75	11.5	11.0	5.0	2416	2480		0.81	85	27.3	14
2.00	2.05	10.65	10.65	11.75	10.8	6.0	2425	2660		0.8	83	26.5	14
2.02	2.07	10.8	10.5	11.8	10.6	7.0	2416	2710		0.8	80	24.0	14
2.075	2.13	10.9	10.3	11.9	10.5	8.0	2422	2770		0.8	75	22.5	14
2.057	2.15	10.93	10.2	11.97	10.35	9.0	2422	2830		0.8	75	22.5	14
2.05	2.13	11.0	10.1	12.0	10.3	10.0	2426	2910		0.8	75	22.0	14
2.057	2.3	11.03	10.0	12.05	10.15	11.0	2430	2960		0.8	75	21.3	14
2.12	2.5	11.1	9.97	12.1	10.1	12.0	2434	3060		0.8	75	21.0	14
2.19	2.9	11.1	9.9	12.1	10.0	13.0	2435	3140		0.8	75	20.5	14
2.4	2.5	11.15	9.8	12.15	9.95	14.0	2435	3210		0.8	72	20.0	14

[a]Test Series No. 16

Total load on the bearing is:

$$P = 14.5W + 27.13$$
$$= 27.13 \text{ lb.} \quad (37)$$

Here, 14.5 is the loading-arm ratio, and 27.13 is the combined weight of the test bearing, the loading arm and the loading pad. Unit load on each short bearing is:

$$PUNIT = P/(m\ a\ d)$$
$$= 27.13/(8 \times 0.1667 \times 2.4842)$$
$$= 8.189 \text{ lb.} \quad (38)$$

Length-to-diameter ratio is:

$$RLTD = (0.1667)/(2.4842)$$
$$= 0.0671. \quad (39)$$

Diameter-to-diameter-clearance ratio is:

$$DTCD = d/c_d$$
$$= 477.77. \quad (40)$$

Film thickness measured by sensing element 1 is:

$$FILMT1 = (VDD1-6.2)/1000$$
$$= 0.00272 \text{ inch.} \quad (41)$$

Similarly,

$$FILMT2 = (VDD2-5.4)(0.0052)/(11.4-5.4)$$
$$= 0.00390 \text{ inch.} \quad (42)$$

$$FILMT3 = (VDD3-6.3)(0.0052)/(12.4-6.3)$$
$$= 0.00281 \text{ inch.} \quad (43)$$

$$FILMT4 = (VDD4-5.4)(0.0052)/(11.6-5.4)$$
$$= 0.0041 \text{ inch.} \quad (44)$$

Change in radial clearance due to thermal expansion is:

$$CHINRC = (TEMPAV-70)(6.2545 \times 10^{-6})/2$$
$$= (0.7946 \times 10^{-4}) \text{ inch.} \quad (45)$$

Film thicknesses corrected to room temperature are:

$$FILMTC1 = FILMT1-CHINRC$$
$$= 0.00264 \text{ inch.} \quad (46)$$

$$FILMTC2 = 0.00382 \text{ inch.} \quad (47)$$

$$FILMTC3 = 0.00273 \text{ inch.} \quad (48)$$

$$FILMTC4 = 0.00403 \text{ inch.} \quad (49)$$

Average film thickness at shaft bottom is:

$$FILMTA1 = (FILMTC1 + FILMTC3)/2$$
$$= 0.00268 \text{ inch.} \quad (50)$$

Average film thickness at 90° from shaft bottom line is:

$$FILMTA2 = (FILMTC2 + FILMTC4)/2$$
$$= 0.00392 \text{ inch.} \quad (51)$$

Average eccentricity ratio at operating temperature is:

$$\text{ECRATA} = \sqrt{(\text{FILMTA1-c})^2 + (\text{FILMTA2-c})^2}/(\text{c} + \text{CHINRC})$$

$$= 0.4957. \tag{52}$$

Tangent of attitude angle is:

$$\text{TANGPA} = (\text{FILMTA2-c})/(\text{FILMTA1-c})$$

$$= 15.218. \tag{53}$$

Attitude angle is:

$$\text{PHI} = \text{Arc tan (TANGPA)}$$

$$= 86.24 \text{ degrees}. \tag{54}$$

From Figure 6, page 16, viscosity at TEMPAV = 95.41°F is:

$$\text{VCSITY} = (63.59)(10^{-7}) \text{ Reyns}. \tag{55}$$

Revolution per second is:

$$\text{RPMSEC} = \text{RPM}/60$$

$$= 26. \tag{56}$$

Surface velocity is:

$$U = \pi d(\text{RPMSEC})$$

$$= 203 \text{ inch/sec}. \tag{57}$$

Sommerfeld number is:

$$\text{SOMMER} = (\text{VCSITY})(\text{RPMSEC})(\text{DTCD})^2/\text{PUNIT}$$

$$= 4.607. \tag{58}$$

Capacity number is:

$$\text{CAPANO} = (\text{SOMMER})(\text{RLTD})^2$$

$$= 0.0207. \tag{59}$$

Load number is:

$$\text{RLOAD} = 1/\text{CAPANO}$$

$$= 48.19. \tag{60}$$

Friction force is:

$$\text{FRFORC} = \frac{(2 \times 5.97)(\text{E-STRANI})}{(122 \times 4.536)(\text{md})}$$

$$= 0.601 \text{ lb}. \tag{61}$$

Petroff friction force is:

$$\text{FRPTRF} = 2\pi^2 \text{ a d (VCSITY)(RPMSEC)(DTCD)}$$

$$= 0.645. \tag{62}$$

Friction ratio is:

$$\text{FRRATI} = (\text{FRFORC})/(\text{FRPTRF})$$

$$= 0.931. \tag{63}$$

Friction variable is:

$$\text{FRVARI} = m(\text{FRFORC})(\text{DTCD})(\text{RLTD})^2/P$$
$$= 0.381. \tag{64}$$

Flow rate at TEMPS = 68.72°F and float indication 14 is:

$$\text{FLOW RATE} = 45.97 \text{ cc/min.} \tag{65}$$

Assuming the pressure at oil exit to be atmospheric, the sealing coefficient is:

$$\Lambda = 6(\text{VCSITY})(U\ \ell)/(c^2\ \text{BSP})$$
$$= 22.4. \tag{66}$$

Reynolds number based on clearance is:

$$Re_c = \frac{(2.54)^3}{(453.6 \times 32.2 \times 12)} \quad \frac{U\rho c}{\mu} \quad . \tag{67}$$

From Equation (19), $\rho = 0.862$ gm/cc at TEMPAV = 94.41°F. Thus:

$$Re_c = 6.67. \tag{68}$$

APPENDIX B

CALIBRATION OF FILM THICKNESS MEASUREMENT DEVICE

Figure 19 shows the arrangement in which sensing elements were installed. For all shaft relative motion studies, two sensing elements mounted at 90 degrees radially should suffice to make the measurement. For careful observation of eccentricity, however, two sensing elements were mounted at each end of the bearing. The sensing elements were mounted 0.005 to 0.008 inch away from the bearing surface as shown in Figure 19. When the bearing was kept in the position shown, sensing elements 1 and 3 would indicate some output in volts. This was called initial voltage for zero clearance. Dial indicators mounted on the top of the bearing measured the vertical displacements as the bearing was lifted. Voltage output was recorded for known vertical displacements. In a similar way, sensing elements 2 and 4 were calibrated. Each transducer was adjusted for a scale factor that would render an output of at least 1 volt (on voltmeter) per mil clearance. Figure 20 shows a linear relationship between the voltage output and clearance. In the first phase of the experiment, in which eight test series were conducted, the equations for oil film thickness measurement were found to be:

$$FILMT1 = (VDD1-6.4)/1000. \quad (69)$$

$$FILMT2 = (VDD2-5.8)/1136. \quad (70)$$

$$FILMT3 = (VDD3-6.6)/1174. \quad (71)$$

$$FILMT4 = (VDD4-5.6)/1193. \quad (72)$$

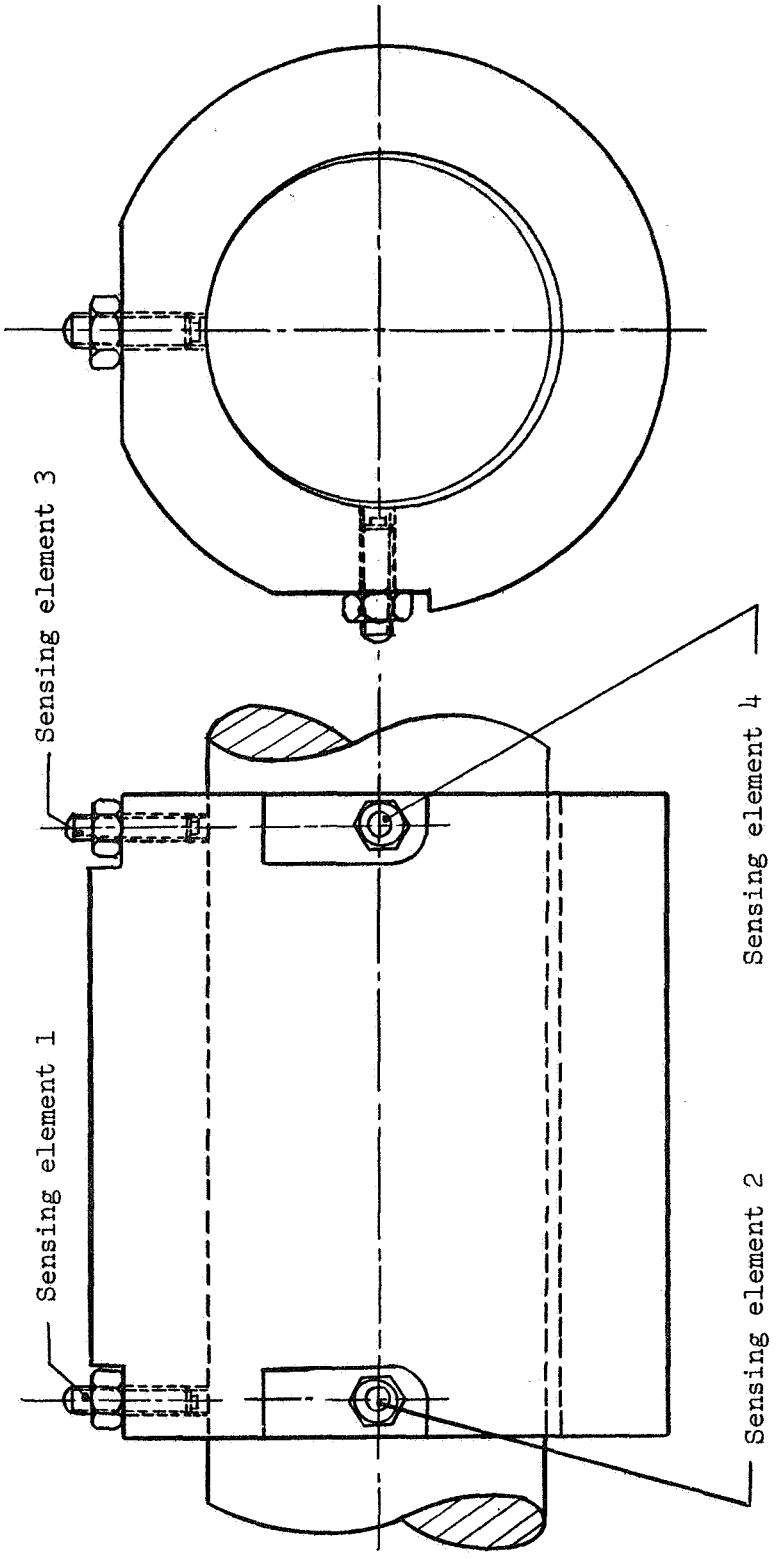

Figure 19. Relative position of sensing elements at the time of calibration.

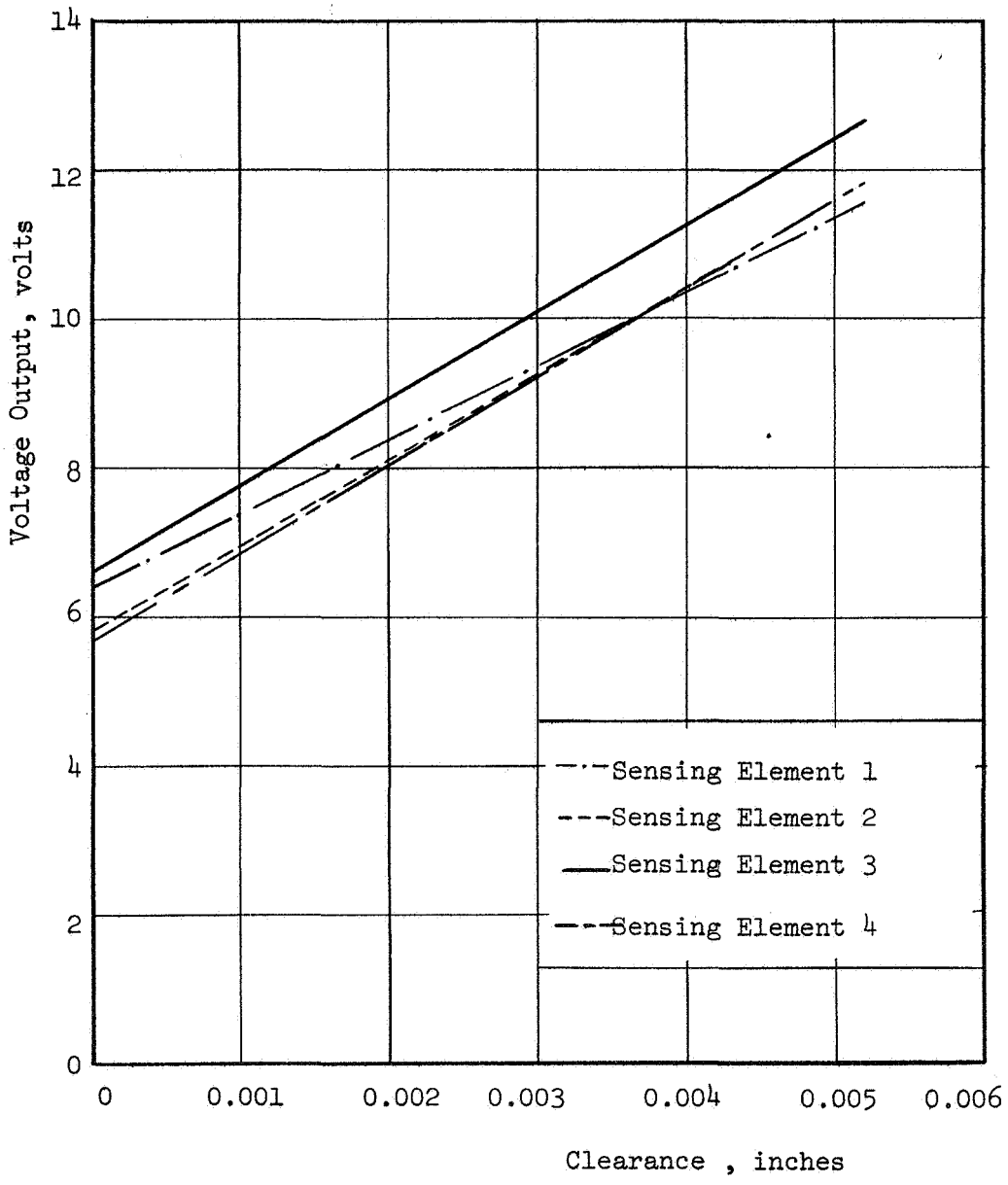

Figure 20. Distance detector voltage output versus bearing clearance.

APPENDIX C

CALIBRATION OF TORQUE BEAM

Figure 7, page 17, presents a perspective view of the torque-beam assembly. To calibrate the beam the torque arm was removed from the holder temporarily, and known weights were applied at the point on the torque beam where the torque arm would sit. Strain corresponding to the known weight was recorded from the strain indicator. Ten readings were taken in this manner. Figure 21 shows the graph of strain versus load on the torque beam. From the graph the average strain per 100 gm. of load was found to be 122 microinch/inch. Thus, if the bearing of diameter d inches and torque-arm length L inches exerts torque, and the strain indicator reads E microinch/inch of strain:

$$T = \frac{(E\text{-STRANI})(100L)}{(122 \times 453.6)} \text{ lb-inch.} \qquad (73)$$

At zero speed of the shaft, E was found to be equal to STRANI.

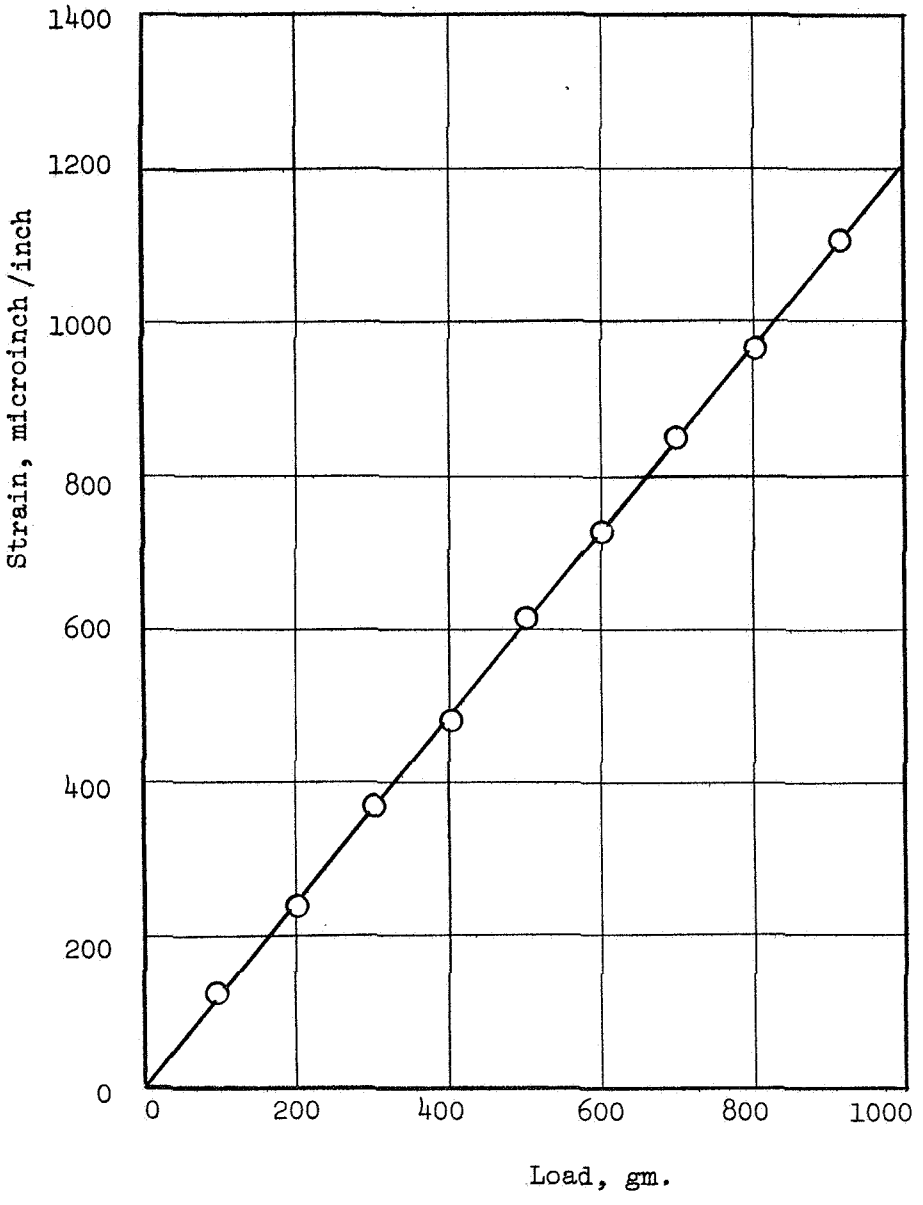

Figure 21. Load versus strain on the torque beam.

APPENDIX D

CALIBRATION OF FLOW METER

The theoretical prediction method for flow meter calibration, suggested by Fischer and Porter [11], gives the following equations:

$$R = A(1.45 \times 10^{-7})\sqrt{(\rho_f - \rho_{OPT})\rho_{OPT}}/\mu_{OPT} \ . \tag{74}$$

$$Q = CB\sqrt{(\rho_f - \rho_{OPT})\ \rho_{OPT}}/\rho_{STP} \ . \tag{75}$$

The values of A, B, and ρ for the flow meter were found from the catalog [11] to be 1142, 434, and 16.6 respectively. Fluid density, ρ_{OPT}, was obtained from Equation (26). Figure 22 describes the float characteristic curves, from which the value of flow coefficient, C, could be picked off for a calculated value of viscous influence number, R, and given scale reading. Then, from Equation (75), the flow rate can be calculated. For example, to find the flow rate at TEMPS = 73.4°F and 20 scale reading for Gulf Harmony 47 Oil:

From Figure 8, page 20, μ_{OPT} = 125.7 Reyns.

From Equation (26), ρ_{OPT} = 0.8684 gm/cc.

From Equation (74) the value of R is found to be:

$$R = (1142 \times 1.45\times10^{-7})\ \sqrt{(16.6-0.8684)(0.8684)}/125.7 \tag{76}$$

$$= 48.77.$$

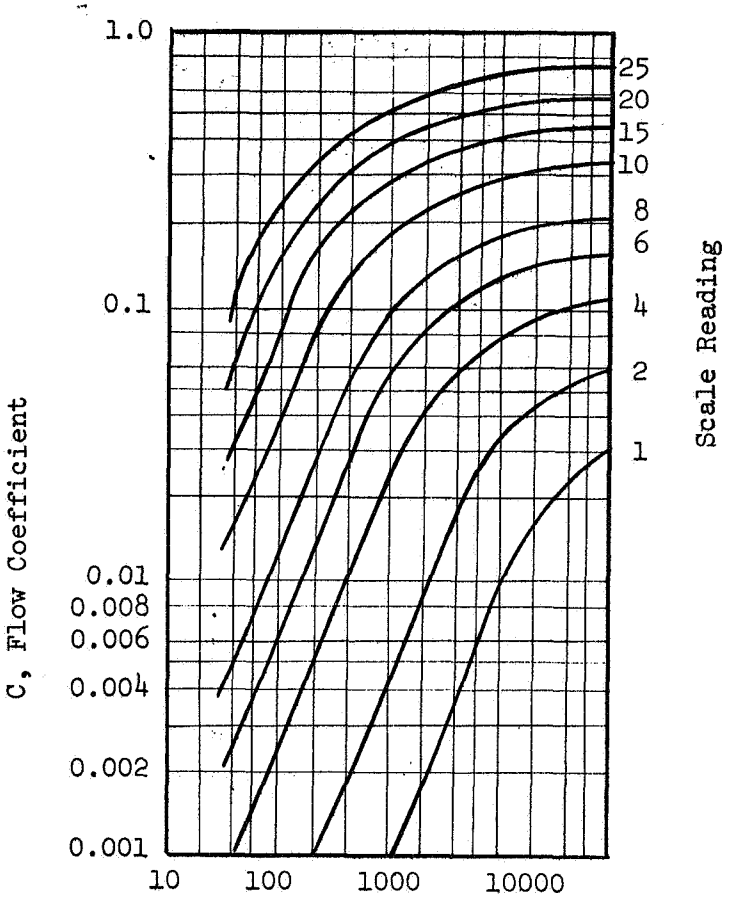

Figure 22. Float characteristic curves reproduced from the catalog by Fischer and Porter, Tri-flat Variable-area Flowmeters, Handbook 10A9010, Warminster: Fischer and Porter Co., January 1964.

From Figure 22, at scale reading 20, and R = 48.77, the value of C is found to be 0.074. From Equation(75) , the flow rate is given by:

$$Q = (0.074 \times 434)\sqrt{(16.6-0.8684)(0.8684)}/0.873$$
$$= 136.04 \text{ std. cc/min.} \qquad (77)$$

A sample calculation sheet for flow rates at scale readings 1 through 25 and a supply temperature of 73 .4°F is presented as follows:

Supply inlet temperature =73.4°F

Density of oil=0.8684 gm/cc

Absolute viscosity=125.7 Reyns

Flow rates in Std.cc/min

Q(1) = 0.1107	Q(10) = 20.645	Q(18) = 105.804
Q(2) = 0.3714	Q(11) = 28.485	Q(19) = 123.728
Q(3) = 0.9210	Q(12) = 34.929	Q(20) = 136.042
Q(4) = 2.0406	Q(13) = 45.133	Q(21) = 152.999
Q(5) = 3.4929	Q(14) = 53.056	Q(22) = 173.357
Q(6) = 5.4452	Q(15) = 65.539	Q(23) = 195.826
Q(7) = 8.1864	Q(16) = 73.463	Q(24) = 217.103
Q(8) =11.3799	Q(17) = 90.958	Q(25) = 237.235.
Q(9) =16.3251		

DISTRIBUTION LIST

Defense Documentation Center
Cameron Station
Alexandria, Virginia 22314

Mr. P. H. Broussard
NASA, R-ASTR-GC
Marshall Space Flight Center
Huntsville, Alabama 35812

Mr. John J. Gurtowski
Naval Air Systems Command
Code AIR 52032C - Dept. of the Navy
Washington, D. C. 20360

Mr. Robert L. Johnson
Chief, Lubrication Research Branch
NASA, Lewis Research Center
Cleveland, Ohio 44135

Mr. W. C. Karl
Office of Naval Research, Code 473
Department of the Navy
Washington, D. C. 20360

Mr. Lawrence P. Ludwig
Head, Seals Section
NASA, Lewis Research Center
Cleveland, Ohio 44135

Mr. Joseph Maltz
Materials Research Program
National Aeronautics & Space Adm.
Washington, D. C. 20546

Col. W. Metscher
Office of Director of Defense Research
and Engineering
Room 3C128, Pentagon
Washington, D. C. 20301

Mr. E. R. Taylor
Reactor Engineering Division
Oak Ridge National Laboratory
Oak Ridge, Tennessee 37830

Mr. Marshall J. Armstrong, Jr.
U. S. Army Mobility Equipment Research
and Development Center
Fort Belvoir, Virginia 22060

Mr. Richard N. Belt
U. S. Army Mobility Equipment Research
and Development Center
Fort Belvoir, Virginia 22060

Mr. Floyd Lux
U. S. Tank Automotive Center
Propulsion Systems Laboratory, SMOTA-RCP.4
Warren, Michigan 48090

Mr. J. R. Crowder
Flight Mechanics & Fluid Systems Section
(AIR 5303)
Naval Air Systems Command - Dept. of the Navy
Washington, D. C. 20360

Mr. Roy R. Peterson
Naval Ship Systems Command (Code 03413)
Department of the Navy
Washington, D. C. 20360

Dr. Earl Quandt
Naval Ship Research & Development Center
Annapolis Division
Annapolis, Maryland 21402

Mr. Alan Schrader
Naval Ship Research & Development Center
Annapolis Division
Annapolis, Maryland 21402

Mr. Lyman Carlyle Fisher
Naval Ordnance Laboratory
Department F (Code 510) - White Oak
Silver Spring, Maryland 20910

Mr. Stanley Doroff
Office of Naval Research (Code 438)
Department of the Navy
Washington, D. C. 20360

Mr. John W. Zmurk
Air Force Aero Propulsion Laboratory (APIP-1)
Wright-Patterson Air Force Base, Ohio 45433

Capt. Kenneth R. Hooks
Air Force Weapons Laboratory WLDC
Kirtland Air Force Base, New Mexico 87117

Dr. Joseph F. Masi
Air Force Office of Scientific Research, SREP
1400 Wilson Boulevard
Arlington, Virginia 22209

Mr. Frank J. Mollura
Rome Air Development Center, EMEAM
Griffiss Air Force Base, New York 13440

Mr. Gerald S. Leighton
SEPO - Division of Space Nuclear Systems
U. S. Atomic Energy Commission
Washington, D. C. 20545

Mr. C. E. Miller, Jr.
Division Reactor Development & Technology
U. S. Atomic Energy Commission
Washington, D. C. 20545

Bureau of Naval Personnel
Department of the Navy
Washington, D. C. 20370
Attn: Technical Library

Naval Air Systems Command
Department of the Navy
Washington, D. C. 20360
Attn: Technical Library Division, AIR-604

Naval Applied Science Laboratory
Flushing and Washington Avenues
Brooklyn, New York 11251
Attn: Technical Library, Code 222

U. S. Naval Oceanographic Office
Suitland, Maryland 20390
Attn: Library, Code 1640

U. S. Naval Postgraduate School
Monterey, California 93940
Attn: Library, Code 0212

DISTRIBUTION LIST (Cont'd)

Naval Ship Engineering Center
Philadelphia Division
Philadelphia, Pennsylvania 19112
Attn: Technical Library

Naval Ship Research & Development Center
Annapolis Division
Annapolis, Maryland 21402
Attn: Library, Code A214

Naval Ship Systems Command
Room 1532 Main Navy
Washington, D. C. 20360
Attn: Technical Library

U. S. Atomic Energy Commission
Argonne National Laboratory
9700 South Cass Avenue
Argonne, Illinois 60440
Attn: Library

National Bureau of Standards
Washington, D. C. 20025
Attn: Library

Battelle Memorial Institute
505 King Avenue
Columbus, Ohio 43201
Attn: Library

Massachusetts Institute of Technology
Cambridge, Massachusetts 02139
Attn: Library

Naval Undersea Warfare Center
3202 East Foothill Boulevard
Pasadena, California 91107
Attn: Technical Library

Navy Underwater Sound Laboratory
Fort Trumbull
New London, Connecticut 06320
Attn: Technical Library

U. S. Naval Weapons Laboratory
Dahlgren, Virginia 22448
Attn: Technical Library

The Franklin Institute
Benjamin Franklin Parkway at 20th Street
Philadelphia, Pennsylvania 19103
Attn: Library

Power Information Center
University City Science Institute
3401 Market Street, Room 2107
Philadelphia, Pennsylvania 19104

Aerojet-General Corporation
Von Karman Center
Azusa, California 91702
Attn: Library

Aerojet-General Nucleonics
San Ramon, California 94583
Attn: Library

University of Arizona
Department of Aerospace and
Mechanical Engineering
Tucson, Arizona 85721
Attn: Professor Kececioglu

AiResearch Manufacturing Company
9851 Sepulveda Boulevard
Los Angeles, California 90045
Attn: Library

AiResearch Manufacturing Company
402 South 36th Street
Phoenix, Arizona 85034
Attn: Library

General Electric Company
Flight Propulsion Division
Cincinnati, Ohio 45215
Attn: Library

General Electric Company
Mechanical Technology Laboratory
Research and Development Center
Schenectady, New York 12301
Attn: Library

UNCLASSIFIED

Security Classification

DOCUMENT CONTROL DATA - R & D

(Security classification of title, body of abstract and indexing annotation must be entered when the overall report is classified)

1. ORIGINATING ACTIVITY (Corporate author)	2a. REPORT SECURITY CLASSIFICATION
University of Tennessee Knoxville, Tennessee William K. Stair, Mech. & Aero. Engr. Dept.	Unclassified
	2b. GROUP --

3. REPORT TITLE

An Experimental Study of the Viscoseal Bearing

4. DESCRIPTIVE NOTES (Type of report and inclusive dates)

Interim - February 1969

5. AUTHOR(S) (First name, middle initial, last name)

Chandrakant Khumaji Shah

6. REPORT DATE	7a. TOTAL NO. OF PAGES	7b. NO. OF REFS
February 1969	63	12

8a. CONTRACT OR GRANT NO.	9a. ORIGINATOR'S REPORT NUMBER(S)
NGR-43-001-003 and N00014-68-A-0144 b. PROJECT NO.	ME 69-T57-2
c. d.	9b. OTHER REPORT NO(S) (Any other numbers that may be assigned this report) --

10. DISTRIBUTION STATEMENT

This document has been approved for public release and sale; its distribution is unlimited.

11. SUPPLEMENTARY NOTES	12. SPONSORING MILITARY ACTIVITY
--	-

13. ABSTRACT

The experimental data obtained from two groove geometries of the viscoseal bearing were analysed to study the bearing characteristics and the sealing performance. The experimental bearing characteristics were compared with the Dubois and Ocvirk Short-bearing Approximation. The sealing performance analysis of the bearing included (1) the determination of the sealing coefficient which was compared with the Stair and Hale method of theoretical prediction and (2) the effect of the bearing eccentricity ratio on the sealing coefficient, which was compared with the Vohr and Chow method of theoretical prediction.

The results of the study indicated that, at constant load and speed, the bearing supply pressure had no effect on the bearing eccentricity ratio; at a constant flow rate, however, the bearing supply pressure decreased as the bearing eccentricity ratio increased. Except for the shaft center locus findings, the experimental results were in fair agreement with the Short-bearing Approximation. The experimental results showed good agreement with a numerical analysis of the viscoseal bearing. The study also indicated that an increase in the land width resulted in an increase in the load-carrying capacity of the bearing. The experimental sealing coefficient did not agree with the theoretical preduction, although the results indicated that the sealing coefficient increased with an increase in the bearing eccentricity ratio.

14. KEY WORDS	LINK A		LINK B		LINK C	
	ROLE	WT	ROLE	WT	ROLE	WT
Bearing, Lubrication, Viscoseal, Sealing, Oil Groove						